

A POLYMERIC IMPLANT FOR LUMBAR BONE DEFECTS

A THESIS SUBMITTED TO
THE GRADUATE SCHOOL OF NATURAL AND APPLIED SCIENCES
OF
MIDDLE EAST TECHNICAL UNIVERSITY

BY

BÜŞRA GÜNAY

IN PARTIAL FULFILLMENT OF THE REQUIREMENTS
FOR
THE DEGREE OF MASTER OF SCIENCE
IN
BIOTECHNOLOGY

SEPTEMBER 2015

Approval of the thesis:

A POLYMERIC IMPLANT FOR LUMBAR BONE DEFECTS

submitted by **BÜŞRA GÜNAY** in partial fulfillment of the requirements for the degree of **Master of Science in Biotechnology Department, Middle East Technical University** by,

Prof. Dr. Gülbin Dural Ünver
Dean, Graduate School of **Natural and Applied Sciences**

Prof. Dr. Filiz Bengü Dilek
Head of Department, **Biotechnology**

Prof. Dr. Vasif Hasırcı
Advisor, **Biological Sciences Dept., METU**

Prof. Dr. Nesrin Hasırcı
Co-advisor, **Chemistry Dept., METU**

Examining Committee Members:

Prof. Dr. Filiz Bengü Dilek
Environmental Engineering Dept., METU

Prof. Dr. Vasif Hasırcı
Biological Sciences Dept., METU

Prof. Dr. Alpaslan Şenköylü
Department of Orthopedics and Traumatology, Gazi University

Assoc. Prof. Dr. Can Özen
Biotechnology Dept., METU

Asst. Prof. Dr. Ergin Tönük
Mechanical Engineering Dept., METU

Date: 08.09.2015

I hereby declare that all information in this document has been obtained and presented in accordance with academic rules and ethical conduct. I also declare that, as required by these rules and conduct, I have fully cited and referenced all material and results that are not original to this work.

Name, Last Name : Büşra Günay

Signature :

ABSTRACT

A POLYMERIC MATERIAL FOR LUMBAR BONE DEFECTS

Günay, Büşra
MS., Department of Biotechnology
Advisor: Prof. Dr. Vasıf Hasırcı
Co-advisor: Prof. Dr. Nesrin Hasırcı

September 2015, 71 pages

This thesis aims to develop a polymeric composite material that can be used as a lumbar fusion cage material. Lumbar fusion cages are one of the devices used in spinal fusion procedures for some spinal disorders such as spondylosis and degenerative disc disease that may occur due to age, trauma or genetic reasons. These devices are most frequently made of metals (e.g. titanium) and polymers (e.g. PEEK). The mechanical properties of such a device should not be much higher than that of the bone so that stress shielding does not lead to defective healing. It should have proper interaction with the cells to achieve high fusion rates.

In order to develop a material for such a device, poly(methylmethacrylate) (PMMA) and hydroxyapatite (HAp) are compounded together in varying ratios and molded into plates using hot melt extrusion and injection molding. The plates were tested to assess the mechanical properties and *in vitro* to determine the changes in cell morphology and rate of proliferation of human osteoblast-like (HOB) cells. It was found that the mechanical properties of PMMA were significantly improved with increasing amount of HAp. HOB cells responded to the increasing HAp content and roughness of the surfaces with

increased proliferation and presented filopodia indicating good interaction with the plate surface. The optimum HAp content for use as a fusion cage is around 20-30% (w/w). It was concluded that PMMA can be compounded with HAp successfully to yield a good material for use in spinal fusion studies.

Keywords: Poly(methylmetacrylate) (PMMA), Hydroxyapatite (HAp), Hot Melt Extrusion, Injection Molding, Spinal Fusion Cages

ÖZ

LUMBAR KEMİK DEFEKTLERİ İÇİN POLİMERİK İMPLANT

Günay, Büşra
Yüksek Lisans, Biyoteknoloji Bölümü
Tez Yöneticisi: Prof. Dr. Vasıf Hasırcı
Ortak Tez Yöneticisi: Prof. Dr. Nesrin Hasırcı

Eylül 2015, 71 sayfa

Bu tezin amacı lumbar füzyon kafesi malzemesi olarak kullanılabilen polimerik kompozit bir malzeme oluşturmaktır. Lumbar füzyon kafesleri, yaş ve travmaya bağlı ya da kalıtsal olarak görülebilen spondilit ve dejeneratif disk hastalığı gibi problemlerin tedavisinde omurga füzyon ameliyatlarında kullanılan donanımlardan biridir. Bu kafesler çoğunlukla metallerden (ör. titanyum) veya polimerlerden (ör. PEEK) yapılır. Böyle bir malzemenin mekanik özelliklerinin, kemiğinkinden fazla olmaması gerekir. Hücrelerle etkileşimi, yüksek füzyon oranları elde etmek için yeterli düzeyde olmalıdır.

Anlatılan koşullarda bir malzeme üretmek için çeşitli miktarlarda poli(metilmetakrilat) (PMMA) ve hidroksiapatit (HAp) sıcak ekstrüzyon ve enjeksiyon kalıplama yöntemi kullanılarak karıştırılmış ve plaka haline getirilmiştir. Plakaların mekanik özelliklerinin araştırılması ve insan kemik hücrelerinin bu plakalar üzerinde morfoloji ve hücre artışı açısından değerlendirilmesi için mekanik ve *in vitro* testler yapılmıştır. Bu deneylerin sonucunda, HAp miktarı arttıkça PMMA'nın mekanik özelliklerinin de anlamlı bir biçimde arttığı görülmüştür. Hücrelerin artan HAp miktarına ve yüzey pürüzlülüğüne, yüzeyle etkileşiminin iyi olduğu anlamına gelen artan hücre bölünmesiyle ve filopod oluşturarak tepki verdikleri görülmüştür. Füzyon kafesi olarak kullanılması için en uygun HAp içeriği %20-30 civarındadır. Sonuç olarak, PMMA'nın HAp ile başarılı bir şekilde

karıştırılarak omurga füzyon çalışmalarında kullanılabilir uygun bir malzeme oluşturabileceği görülmüştür.

Anahtar Kelimeler: Poli(metilmetakrilat) (PMMA), Hidroksiapatit (HAp), Sıcak Ekstrüzyon, Enjeksiyon Kalıplama, Omurga Füzyon Kafesleri

ACKNOWLEDGEMENTS

I would like to express my gratitude to many people involved in this work in some way or another; I cannot overlook the contribution they made.

First of all, I am grateful to my advisor Prof. Dr. Vasif Hasircı who always had a stern look about him but had been an exceptional advisor to me with timely guidance in the right direction, insights and encouragement when most needed. It is an honor to have the opportunity of being the student of such an academic. I also thank my co-advisor Prof. Dr. Nesrin Hasircı for her valuable advice and remarks.

I would also like to thank the collaborator of the MIGEP project, Doratek Medical Group, for the financial support as well as the opportunity to make this work industrial in the future.

My sincere thanks for the both expected and unforeseen (though much appreciated) help coming from METU-BIOMATEN with sufficient amount of bossiness, academic advice, sympathy, patience and understanding of my not-so-businesslike lab mates; Selcen Alagöz, Ezgi Antmen, Damla Arslantunalı, Gökhan Bahçecioglu, Cemile Kılıç Bektaş, Deniz Sezlev Bilecen, Senem Büyüksungur, Tuğba Dursun, Gözde Eke, Mehmet Nizamoğlu, Esen Sayın, Ayla Şahin and, in jest, honorary member Çiğdem Yılmaz with an addition of Menekşe Ermiş Şen for her confocal work as well as last minute saves from major emotional breakdown and Arda Büyüksungur for also his confocal and microCT work. I would also like to thank our technician Zeynel Akın for his practical solutions to almost everything.

My everlasting thanks belong to Bensus Tunca, Bilge Sürün and Övsev Dörtlemmez for just being there, though mostly away, for the last 12 years and keeping it up until the last 12 minutes of this work.

Last but not the least, I deeply thank Cem Yolaçan for his unbelievable level of understanding and, of course, my ever more supportive parents Tülin Günay and Özcan Günay, who and I cannot always understand one another but try to do our best at all times.

TABLE OF CONTENTS

ABSTRACT	v
ÖZ.....	vii
ACKNOWLEDGEMENTS	ix
TABLE OF CONTENTS	ixi
LIST OF FIGURES	xiv
LIST OF TABLES	xvi
LIST OF ABBREVIATIONS	xvii
1. INTRODUCTION.....	1
1.1. Structure of the Bone and Related Disorders.....	1
1.1.1. Structure of the Bone.....	1
1.1.2. Mechanical Properties of the Bone.....	4
1.1.3. Formation of the Bone.....	7
1.1.4. Bone Related Disorders	8
1.2. Degenerative Lumbar Spinal Disorders.....	9
1.2.1. Spinal Stenosis.....	10
1.2.2. Spondylosis.....	11
1.2.3. Lumbar Herniation	11
1.2.4. Scoliosis.....	12
1.2.5. Lumbar Degenerative Disc Disease	13
1.3. Treatment of Lumbar Spinal Disorders	13
1.3.1. Non-operative Treatments	13

1.3.2.	Operative Treatments.....	14
1.4.	Lumbar Cages	18
1.4.1.	Materials Used in Lumbar Cages.....	20
1.4.2.	Problems with Current Cage Materials.....	22
1.4.3.	Poly(methylmethacrylate) (PMMA) and its use in Medical Devices.....	24
1.5.	Aim and Novelty of the Study.....	25
2.	MATERIALS AND METHODS.....	27
2.1.	Materials.....	27
2.2.	Methods.....	27
2.2.1.	Preparation of PMMA-HAp Composites.....	27
2.2.1.1.	Compounding and Extrusion of PMMA and HAp.....	27
2.2.1.2.	Injection Molding of the Composites	28
2.2.2.	Characterization of the PMMA-HAp Composites.....	29
2.2.2.1.	MicroCT imaging	29
2.2.2.2.	Mechanical Testing.....	29
2.2.2.3.	Scanning Electron Microscopy (SEM) and Energy Dispersed X-Ray (EDX) Analysis	31
2.2.2.4.	Surface Profilometry.....	32
2.2.2.5.	Contact Angle	32
2.2.3.	<i>In vitro</i> Studies.....	33
2.2.3.1.	Isolation of Human Osteoblast-like (HOB) Cells.....	33
2.2.3.2.	HOB Cell Culture	33
2.2.3.3.	Cell Seeding on PMMA-HAp Composites	34
2.2.3.4.	Cell Viability Assay.....	34
2.2.3.5.	Microscopic Characterization of HOB Cells.....	35

2.2.3.5.1. Confocal Laser Scanning Microscopy	35
2.2.3.5.2. Scanning Electron Microscopy Analysis.....	36
2.2.3.6. Alizarin Red Staining.....	36
2.2.4. Statistical Analysis	36
3. RESULTS AND DISCUSSION.....	37
3.1. Preparation and Characterization of PMMA-HAp Composite Plates	37
3.1.1. Distribution of HAp Particles in PMMA.....	37
3.1.2. Mechanical Properties	39
3.1.2.1. Tensile Properties.....	40
3.1.2.2. Compressive Properties.....	43
3.1.3. Scanning Electron Microscopy Analysis.....	45
3.1.4. Surface Profiles	47
3.1.5. Contact Angle.....	48
3.2. <i>In vitro</i> Studies.....	50
3.2.1. Cell Attachment and Proliferation.....	50
3.2.2. Cell Morphology and Spreading	53
3.2.2.1. Scanning Electron Microscopy and Energy Dispersed X-Ray (EDX) Analysis	53
3.2.2.2. Confocal Laser Scanning Microscopy (CLSM) Analysis.....	55
3.2.3. Staining of Calcium.....	59
4. CONCLUSION	61
REFERENCES	63
APPENDICES	71
APPENDIX A	71

LIST OF FIGURES

FIGURES

Figure 1.1 The organization of the long bone.....	2
Figure 1.2 Examples of stress-strain curve of the bone.....	5
Figure 1.3 Representative stress-strain curve of the cortical bone under tension.....	7
Figure 1.4 Anatomy of the lumbar spine.	10
Figure 1.5 Some examples of the intervertebral disc problems including hernia and degenerated disc.....	12
Figure 1.6 Model of some spinal fusion devices.	16
Figure 1.7 Some of the spinal fixation devices which includes plates, pedicle screw systems, rod and screw systems.	17
Figure 1.8 Chemical structure of poly(methylmethacrylate) (PMMA).....	25
Figure 2.1 The two devices used to produce used to produce pure PMMA and PMMA-HAp composite plates.	28
Figure 2.2 Injection molded PMMA-HAp composite samples..	29
Figure 2.3 Dimensions of a dog bone sample suitable for testing according to ISO 527 standard for tensile test.....	31
Figure 2.4 Characteristic stress-strain curve of pure PMMA..	31
Figure 2.5 The contact angle of a liquid with a substrate gives the wettability of the surface.....	33
Figure 3.1 MicroCT images of PMMA samples carrying varying amounts of HAp.	38
Figure 3.2 Characteristic stress-strain curves for pure PMMA and PMMA-HAp composites under tension.....	41
Figure 3.3 Elastic moduli of the pure PMMA and PMMA-HAp composites, cortical and trabecular bones (Wagoner Johnson & Herschler, 2011), lumbar vertebra (Saha & Pal, 1984), and PEEK (Harper, 2000).	42

Figure 3.4 Compressive properties of some bone samples and cage materials.....	44
Figure 3.5 SEM images of PMMA and PMMA-HAp plates.	46
Figure 3.6 Analysis of surface roughness produced by optical surface profiler..	48
Figure 3.7 Water contact angles for pure PMMA and PMMA-HAp composites.	50
Figure 3.8 Attachment and proliferation of HOB cells on pure PMMA and PMMA- HAp composite plates over 14 days obtained by using the Alamar Blue test.	52
Figure 3.9 SEM micrographs of pure PMMA and 20% (w/w) PMMA-HAp composite plates.	54
Figure 3.10 Energy dispersed X-ray (EDX) analysis of pure PMMA and 20% PMMA-HAp plates with and without HOB cells.....	55
Figure 3.11 CLSM images of HOB cells on pure PMMA and on 20% and 40% PMMA-HAp composite plates on Day 3 and 7.....	57
Figure 3.12 Representative CLSM images of HOB cells.....	58
Figure 3.13 Staining of Ca ⁺² with Alizarin Red of PMMA and PMMA-HAp plates, with and without cells.....	59
Figure A.1 Standard curve for Alamar Blue assay for human osteoblast (HOB) cells.....	59

LIST OF TABLES

TABLES

Table 1.1 Mechanical properties of cortical and trabecular bones and articular cartilage...	6
Table 1.2 Some selected commercially available fusion cages. Almost all are produced from titanium alloy and PEEK.....	19
Table 3.1 Summary of the some tensile and compressive properties of the materials used in this study, PEEK and bone.....	40

LIST OF ABBREVIATIONS

ALIF	Anterior Lumbar Interbody Fusion
ASTM	American Society for Testing and Materials
BMPs	Bone Morphogenetic Proteins
BSA	Bovine Serum Albumin
CaP	Calcium Phosphate
CLSM	Confocal Laser Scanning Microscopy
CT	Computed Tomography
DBM	Demineralized Bone Matrix
DDD	Degenerative Disc Disease
DMEM	Dulbecco's Modified Eagle Medium
DMSO	Dimethyl Sulfoxide
EDTA	Ethylenediamine tetraacetic acid
EDX	Energy Dispersed X-Ray
EtOH	Ethyl alcohol
FBS	Fetal Bovine Serum
FDA	Food and Drug Administration
FITC	Fluorescein isothiocyanate
HAp	Hydroxyapatite

HOB	Human Osteoblasts
IVD	Intervertebral Disc
MSCs	Mesenchymal Stem Cells
MTT	(3-(4,5-Dimethylthiazol-2-yl)-2,5-Diphenyltetrazolium Bromide)
PBS	Phosphate Buffer Saline
PCL	Poly(caprolactone)
PDLLA	Poly(L-lactide-co-D,L-lactide)
PEEK	Polyetheretherketone
PFA	Paraformaldehyde
PLIF	Posterior Lumbar Interbody Fusion
PLLA	Poly(L-lactic acid)
PMMA	Poly(methylmethacrylate)
SEM	Scanning Electron Microscopy
TCPS	Tissue Culture Polystyrene
T _g	Glass transition temperature
UTS	Ultimate Tensile Strength

CHAPTER 1

INTRODUCTION

1.1. Structure of the Bone and Related Disorders

1.1.1. Structure of the Bone

Bone is a complex organization of cells and molecules with structures ranging from macro-scale to molecular scale. Macroscopically, cortical (compact) bone and trabecular (cancellous) bone comprise the main form of the bone. Cortical bone is a dense structure with 70-90 % calcium phosphate content whereas trabecular bone is a porous structure primarily made up of collagen and less organized calcium phosphate. The mechanical properties of the bone, a natural composite, originates from the mineral phase. The organic phase, on the other hand, coordinates and satisfies the metabolic needs of the tissue (Dhoble *et al.*, 2012). At a smaller scale, however, osteons (Haversian systems) which contain blood vessels in Haversian and Volkmann canals, and lamellae with mineralized collagen fibers that runs in distinctive orientations make up the fundamental structure (Figure 1.1). In the cortical bone, collagen fibrils lie in a parallel fashion and form fibers and sheets, and contribute to the mechanical properties.

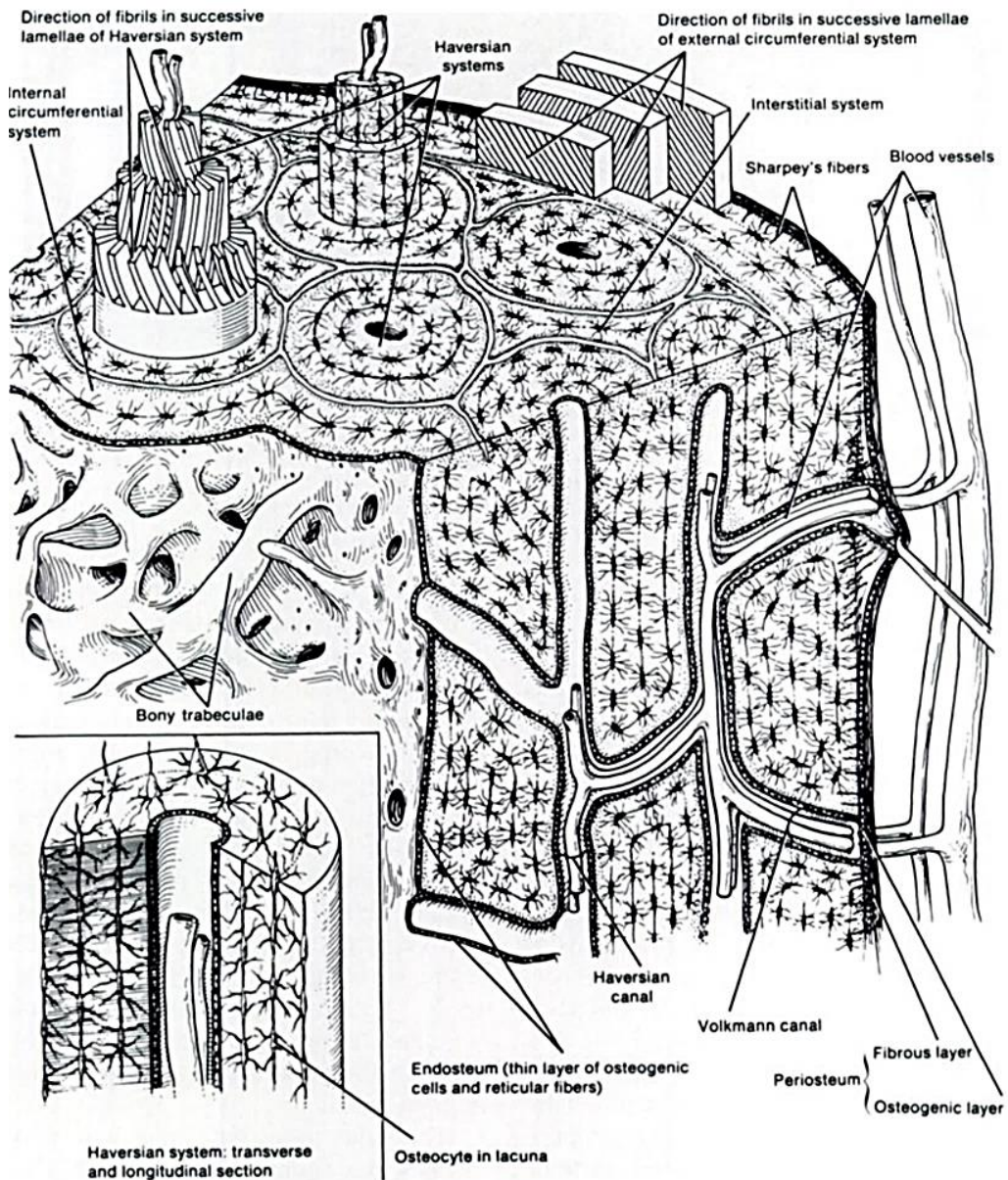


Figure 1.1 The organization of the long bone. Haversian systems are embedded within the bone, appear as oval structures, include Haversian canals with the blood vessels, and the distinctly organized collagen fibrils in the lamellae (Buckwalter *et al.*, 1995).

As the bone consists of hydroxyapatite, collagen and water, the in weight and volume fractions with respect to each other changes with the age, species and function. Primary

functions of the bone are to provide structural foundation, mechanical strength as well as mobility to the body. It also regulates pH of the blood, homeostasis, and mineral, mainly calcium and phosphate, levels for the metabolic processes (Sowjanya *et al.*, 2013; Venkatesan *et al.*, 2015).

Bone tissue serves as a store for calcium and phosphate ions protect delicate organs such as brain, heart and lungs, and provide a stiff skeleton for mobility (Mellon & Tanner, 2012). The minerals, mainly hydroxyapatite, are very active on the surface, have excellent biocompatibility with the bone tissue, and lead to high osteoconductivity. Mineralization does not occur through a chemical reaction but a phase transition. Solid calcium phosphate ($(Ca_{10}(PO_4)_6(OH)_2)$) is formed from soluble calcium and phosphate in the organic matrix, and occurs as a barely crystalline apatite, which becomes more crystalline in time (Buckwalter *et al.*, 1995). The typical Ca:P molar ratio of hydroxyapatite is 1.67.

As stated, bone structure consists of an organic matrix of collagen, water and inorganic minerals as well as a noncollagenous protein matrix, osteoids, and supporting and remodeling cells; namely, osteoblasts, osteocytes and osteoclasts. Osteoblasts, responsible for the mineralization and synthesis of the bone matrix, originate from the undifferentiated mesenchymal stem cells (osteoprogenitor cells). After a stimulus these stem cells differentiate into osteoblasts, migrate and proliferate. The shape of the osteoblast can be flat or plump depending the degree of cellular activity (Kini & Nandeesh, 2012). They also present high levels of alkaline phosphatase which is an enzyme breaking down phosphate. Osteocytes are formed when the osteoblasts differentiate, start to secrete extracellular matrix and eventually embed themselves within it. They comprise most of the cells of the bone structure and through their many filopodia, they serve as mechanosensors governing the osteoblast function. Osteoclasts, on the other hand, do not take part in the bone formation but in the resorption of the bone and are directed by the osteocytes.

The cartilage is a flexible tissue presenting itself around the joints and at the ends of the bones and also found many other parts of the body such as ears, nose, trachea, end of the

ribs and intervertebral discs. It is formed by specialized cells, chondrocytes, and the extracellular matrix they secrete, collagen fibers, proteins, elastic fibers and polysaccharides. It can also mineralize depending on the function. The cartilage tissue does not have blood vessels for the delivery of the nutrients which is supplied by diffusion. There are three types of cartilage, namely, hyaline cartilage, elastic cartilage and fibrocartilage. The most abundant type found in the body is the hyaline cartilage and found at the joints, bronchi and end of the ribs. Elastic cartilage contains elastic fibers providing flexibility as its name suggests and is present at the external ear and larynx. Fibrocartilage is found in the articular cartilage at the end of the joints and in the intervertebral discs (IVD). The outer layer of the IVD, annulus fibrosus, consists of fibrocartilage (Meyer & Weismann, 2006).

1.1.2. Mechanical Properties of the Bone

Bone is the strongest tissue in the body. As the bones are subjected to the mechanical forces, the skeletal design, organic and inorganic contents change accordingly. Modifications and arrangements are made by the cells to meet the new loading requirements. The bone cells identify the mechanical signals and convert them into changes in bone design. This process, simply put, is called bone adaptation (Mellon & Tanner, 2012). The mechanical properties, therefore, depend on the age and the sex of the subject, biological and biomechanical location, chemical composition and highly on the density of the bone.

Since the bone is a highly complex structure and has mechanical properties adapted to the situation, mechanisms for mechanical effects of loads on the bone are either modeled (Bauer *et al.*, 2014) or experimentally evaluated in specific cases. The basic mechanical parameters measured with the bone include, elastic modulus, ultimate strength (under tension, compression and shear), toughness and fracture properties.

There are many reports on the basic mechanical properties of the bone. The mechanical properties of the trabecular bone are lower than that of the cortical bone due to the lower

mineral content, organization, water and polysaccharide content, much higher porosity compared to the cortical bone and to the fact that the structure is not as organized as that of the compact bone (Currey, 1998). Representative stress-strain curves of cortical and trabecular bone are given in Figure 1.2.

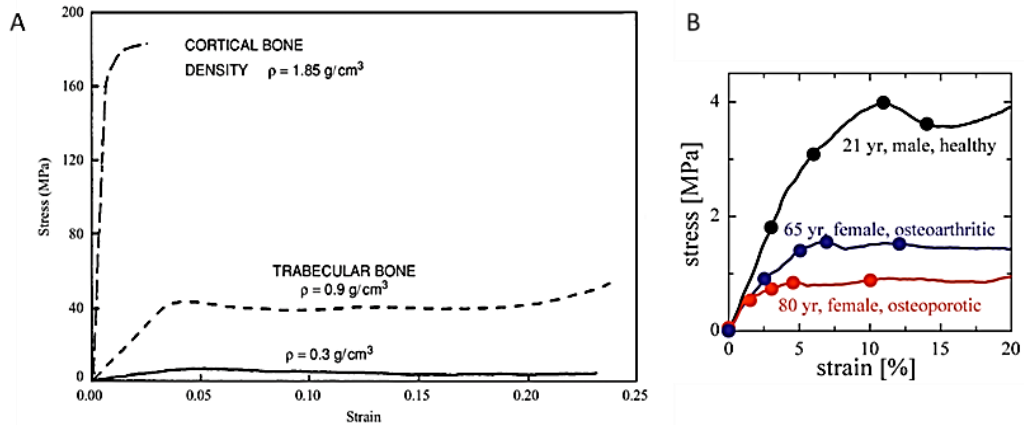


Figure 1.2 Examples of stress-strain curve of the bone. (A) Representative stress-strain curves of cortical and trabecular bone with different densities (Browner, 2009), (B) three samples (one healthy, one osteoarthritic, one osteoporotic) tested in compression by Thurner *et al.* (2005).

The bone has an anisotropic nature which means that it will behave differently depending on whether the force is longitudinal or transverse. Therefore, there are differences in the mechanical properties of the bone due to the direction of the structural orientation as well as the age of the subject and the type, porosity and dryness of the bone. Although there cannot be a single value for any of the properties, certain average values are available (Table 1.1). The elastic modulus of cortical bone is reported to be in the range 50-151 GPa (Wagoner-Johnson & Herschler, 2011), for the trabecular bone, the reported values are in the range 0.6-2 GPa (Mellon & Tanner, 2012). Cortical and trabecular bone were reported to have compressive strengths of 130-180 MPa and 4-12 MPa, respectively (Wagoner-Johnson & Herschler, 2011).

Table 1.1 Mechanical properties of cortical and trabecular bones and articular cartilage.

Property	Cortical Bone		Trabecular Bone		Articular Cartilage	Ref.
	Longitudinal	Transverse	Longitudinal	Transverse		
Compressive Strength (MPa)	130-180		4-12		-	Wagoner-Johnson & Hershler (2011)
	100-230		2-12		-	Hench & Wilson (1993)
	131-224	106-133	3-30	<5	-	Chai <i>et al.</i> (2012)
	205	131	190-209	-	-	Currey (1998)
Tensile Strength (MPa)	50-150		10-20		10-40	Hench & Wilson (1993)
	79-151	51-56	3-20	<5	-	Chai <i>et al.</i> (2012)
	133	53	129-140	-	-	Currey (1998)
Strain to Failure (%)	1-3		5-7		15-50	Hench & Wilson (1993)
Elastic (Young's) Modulus (GPa)	12-18		-		-	Wagoner-Johnson & Hershler (2011)
	17.70	12.80	-		-	Currey (1998)
	-	-	0.6-2		-	Mellon & Tanner (2012)

Even though the values vary to a certain degree there still is a consistency in the numbers. It is observed that the cortical bone is stronger, stiffer and less extensible than trabecular bone. The articular cartilage matches more the properties of cancellous bone.

Whereas the collagen accounts for the toughness of the bone, defined as the energy that it can take up until it breaks, its strength and stiffness comes essentially from the hydroxyapatite $[(Ca_{10}(PO_4)_6(OH)_2)]$ nanocrystals embedded within the structure (Nyman *et al.*, 2006). This can be quantified by calculating the area under the stress- strain curve of the tested material (Figure 1.3). It is, therefore, observed that if the mineral content is higher and the collagen content lower in a bone specimen, the toughness of the bone decreases (Currey, 2014). Similarly, more mineral in the structure of the bone results in a higher strength as well as modulus.

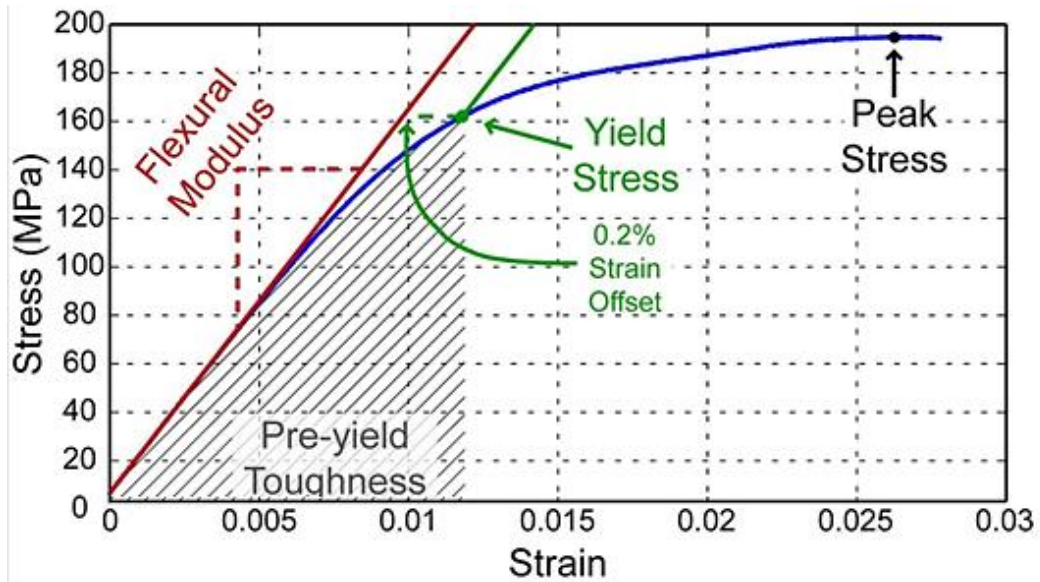


Figure 1.3 Representative stress-strain curve of the cortical bone under tension. Some mechanical parameters are indicated on the curve. Toughness is calculated as the area under the curve as the tangent drawn, yield stress is obtained at the 0.2% strain, and flexural (elastic) modulus is the slope of the initial linear part of the curve and peak stress gives the ultimate strength (Horch *et al.*, 2011).

1.1.3. Formation of the Bone

Bone is a dynamic tissue that responds to internal and external stimuli such as physiological and mechanical forces. Bone formation (osteogenesis) and resorption is a constantly occurring process and is called bone remodeling. The strength of the bone is maintained through its adaptation to biomechanical forces which is replacing the damaged or old bone with the new. The remodeling, therefore, the formation of the bone is achieved by the cells of which the bone is comprised. Osteoblasts and the bone matrix is essential for the bone formation which mainly occurs in two processes. Through intramembranous osteogenesis, the new bone formation starts in the primitive connective tissue mostly resulting in flat bones. In endochondral osteogenesis, on the other hand, a model of the new bone to be formed is initially constructed as a precursor and extracellular organic matrix with noncollagenous proteins, osteoids, are synthesized on

it. The osteoids then mineralize depending on the density required, forming the calcified primary new bone. This structure also includes randomly deposited collagen fibers (woven bone) which is then converted into more aligned fibers. The bone needs to be resorbed for remodeling and cells called osteoclasts break down the collagen fibers and remove the matrix, forming cavities for the newly forming bone (Kini & Nandeesh, 2012). This process of resorption and formation continues throughout the lifetime, hence the dynamic structure of the bone tissue.

1.1.4. Bone Related Disorders

There are numerous disorders concerning the bone and it is not possible to make a simple categorization. However, some of the common disorders genetic, metabolic or traumatic, and some do not have a known cause. In general, the balance within the bone is disrupted and this leads to insufficient healing, bone mineral loss, and weakening. Some of the most common disorders include but are not limited to arthritis, fractures, Paget's disease, osteoporosis, Rickets disease and spinal disorders.

Arthritis (the inflammation of the joint) presents itself with pain, swelling and limited movement. It is a chronic, progressive problem and the reasons leading to it is currently not well understood. There are several types of arthritis. For example, osteoarthritis is a degenerative disease causing cartilage to break down and affecting middle-aged and older people and rheumatoid arthritis is a form of autoimmune disorder where the body treats the healthy cells as foreign bodies leading to the inflammation around the joints (Ponsonby *et al.*, 2005).

Fractures occur due to external reasons like trauma and mostly treated either with casts or fixation devices such as plates, pins and rods depending on how the fracture occurred.

Paget's disease is a problem of the bone remodeling, where one or more bones are affected by high bone turnover. Osteoblast activity and the new bone formation increases and deformations such as thickening of the bone may be observed. The treatments generally include pain management and surgical corrections of the deformities if present.

Osteoporosis is also a bone remodeling condition and is very commonly observed. It is characterized by decreased bone mass and impairment of the structure, and causes bone to become fragile. Osteoporosis has two common types arising from two different reasons. It is either a direct result of the aging process, or it is caused by estrogen deficiency in menopausal women. The symptoms include bone and muscle pain, fracture of the bone due to even minor trauma, and collapsed vertebra (Feng & McDonald, 2011).

Rickets disease occurs in early ages and caused by the deficiency of vitamin D, calcium and phosphate. Osteoblast progenitors are directly affected, mineralization is impaired and mineral content of the bone is lost. If the disease occurs before the growth plates form, deformation in the bones are observed.

Spinal disorders include various types of problems with many different reasons. Neck and back pain are two of the most common problems. Some of the causes that can lead to such problems are exhausting activity, trauma, degeneration of the vertebra, infection and tumors. Specific degenerative cases of spinal disorders where they occur in the lumbar region of the spine are discussed in a separate section below.

1.2. Degenerative Lumbar Spinal Disorders

The spine consists of 33 vertebral bodies, 5 of which belong to the lumbar region (Figure 1.4). A vertebral body consists of the hard and dense cortical bone on the outside covering the trabecular bone inside. Between the pairs of vertebral bodies, there are total of 24 intervertebral discs each consisting of three regions. Annulus fibrosus is composed of collagen fibers and surrounds the inner nucleus pulposus which is made of collagen, water and proteins, and is the main part that absorbs the shock of the applied load (Park & Lakes, 2007). Cartilage endplates form an interface between the vertebral bone and the disc itself. The intervertebral disc, therefore, has a cushioning effect allowing a certain degree of flexion, extension and tension to the spine and preventing friction and deformation of the bones. It is estimated that during heavy lifting, lumbar discs are subjected to forces as much as 17 kN (Pereira *et al.*, 2013).

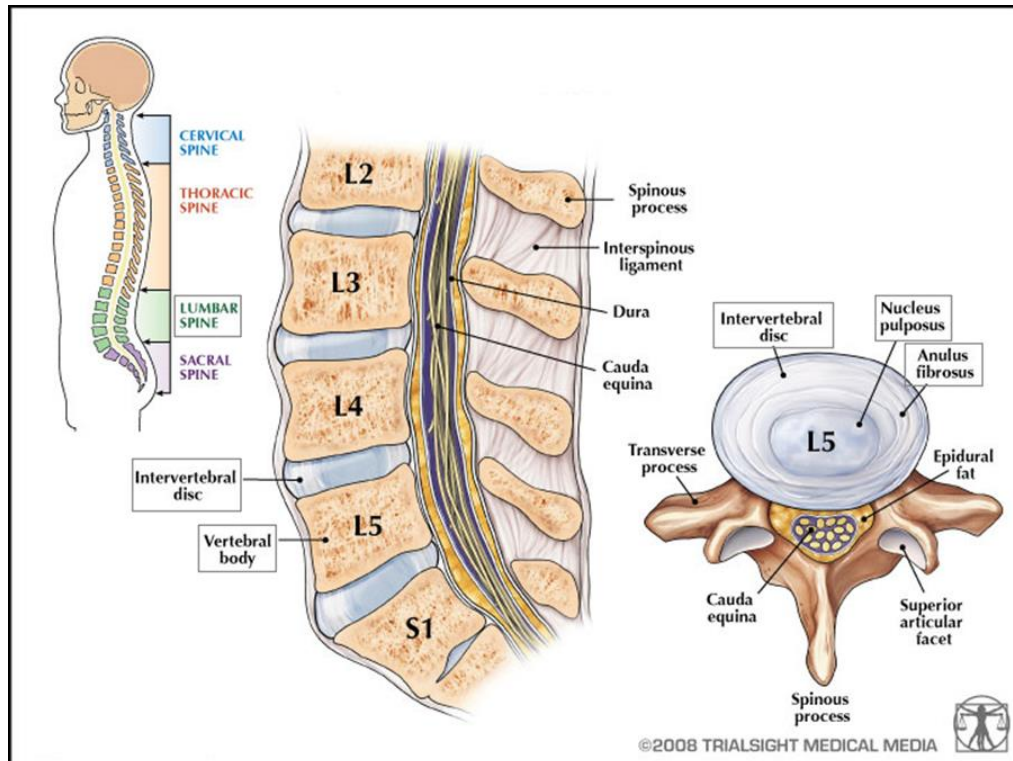


Figure 1.4 Anatomy of the lumbar spine. Between each of the vertebral bodies, intervertebral discs (IVD) are present. IVD has two components; namely, annulus fibrosus and the nucleus pulposus. Retrieved and adapted from <http://www.goudelis.gr/en/content/spine>.

Disorders relating to lower back generally presents themselves with such symptoms as lower back or lower extremity pain. In most such disorders, spine cannot function properly to support the body and enable mobility and motion, reducing the quality of life.

1.2.1. Spinal Stenosis

Stenosis, in general, means the narrowing of the blood vessels. Lumbar stenosis is the narrowing of the lumbar spinal canal, causing compression within; hence, pain in the legs and weakness in the back. Although there is no single cause, contributing factors to

lumbar stenosis includes conditions such as spondylosis and Paget's disease (Andersson & Frymoyer, 1997).

1.2.2. Spondylosis

Spondylosis is defined as the dislocation of one vertebral body on another. In 82 % of the cases, abnormalities occur as the lowest lumbar vertebra (L5) slips forward onto the first sacral vertebra (S1). It can be caused by application of stress causing fatigue fractures, or severe trauma (Andersson & Frymoyer, 1997). It may also occur due to developmental abnormalities or pathological reasons, and in some cases it can be degenerative. Spondylosis manifests itself with lesions, degenerating disc at the site of the slippage and instability of the vertebrae, and the patients often suffer from lower back pain. Degenerative spondylosis occurs due to the degenerative changes of the joints between the vertebra or intervertebral discs, and causes segmental instability.

1.2.3. Lumbar Herniation

Disc herniation refers to the outward shift of the inner part of an intervertebral disc from the surrounding annulus fibrosus (Figure 1.5). As it may happen at all levels of the vertebra, 90-98 % of the surgically treated herniated discs in lumbar region occur at levels L4-L5 and L5-S1 (Byrne *et al.*, 2000). Hernia in the lumbar disc generally is accompanied by lower back pain and may lead to weakness and loss of sensation in lower extremities. As in the case of spondylosis, surgical treatment of the herniated disc is preferred only if the patient does not respond to the physical and drug therapy.

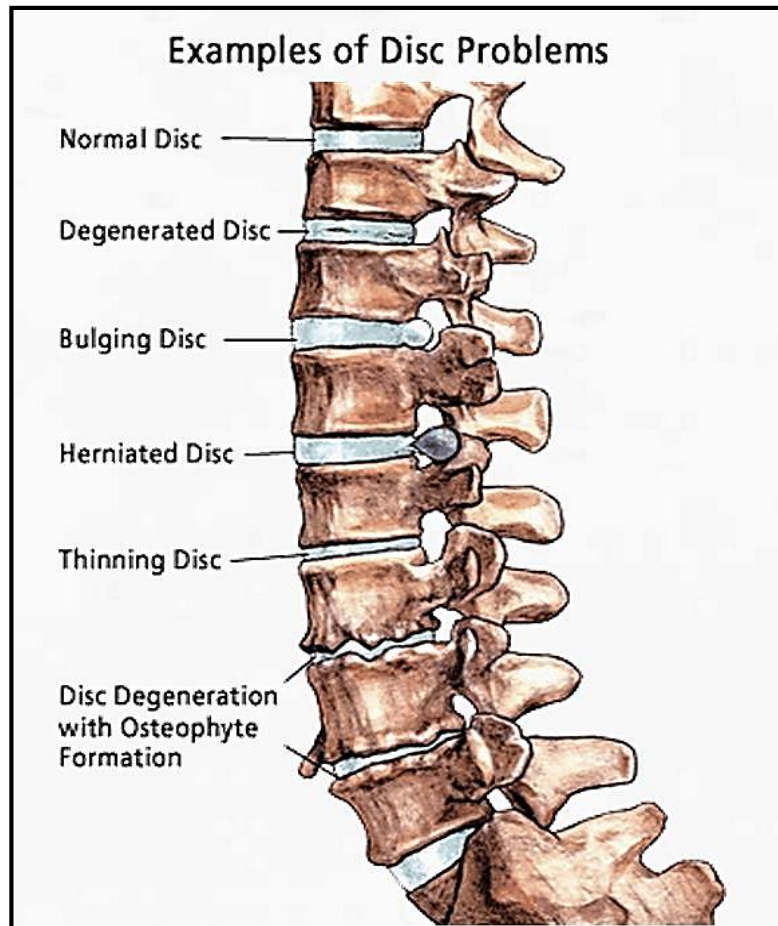


Figure 1.5 . Some examples of the intervertebral disc problems including hernia and degenerated disc. (Retrieved from <http://www.sandiego-spine.com/subject.php?pn=lumbar-disc-disease-035>)

1.2.4. Scoliosis

Adult scoliosis presents itself as the deformity of the vertebrae occurring after the maturation of the skeleton. The deformity generally is congenital and arises before the skeletal maturity and treatment may not be sought before adulthood. It can also be observed *de novo*, in which case it is generally secondary to degeneration of the disc, osteoporosis, or post-operative decompression. Apart from the aesthetic difficulties, back

pain and neurological problems are the most common symptoms observed. As the disease progresses, the curve deteriorates and a new one may develop in some degenerative form.

1.2.5. Lumbar Degenerative Disc Disease

Degenerative disc disease (DDD) is not a separate disease by itself but a generalization of a condition that causes possibly radiating pain and weakness in the spine. There are many reasons that lead to the degeneration of the intervertebral disc, which includes aging, genetic factors and trauma. Mechanical strength of the disc gradually decreases. Later, the degeneration is characterized by the dehydration of the disc (Lipson, 1981). Morphological changes start to occur, the disc is replaced by an amorphous fibrocartilage, disc space narrows due to lack of water content and finally, instability and pain occur (Burkus, 2003). Degeneration generally does not mean the deterioration of the symptoms but the progress of the disc degenerating over time. It was estimated that 11.9 % of the worldwide population is affected by the low back pain and it is a leading cause of disability (Weber *et al.*, 2015).

1.3. Treatment of Lumbar Spinal Disorders

1.3.1. Non-operative Treatments

Almost all chronic, painful spinal disorders share similar non-operative approaches of treatment, which often regard to the pain management and the attempt to increase the quality of life and functionality. Non-operative treatments are widely recommended to avoid the discomfort of a highly invasive surgery. This notion can be preferred as long as there are reports such as that of Smith *et al.* (2014) on the observation that operative treatments are not a better option than non-operative treatments. Schneider *et al.* (2014) argues that the individual therapy with medical care, rehabilitative exercises and group exercises can improve the symptoms of patients with lumbar stenosis as effectively as a surgical treatment. However, there are also studies showing that patients treated surgically have better improvements with respect to pain and functionality compared to those treated non-operatively (Weinstein *et al.*, 2012). Therefore, patients' needs and

problems must be assessed carefully and if the conditions cannot be controlled sufficiently with exercise or pain medication, then invasive surgical options have to be considered.

1.3.2. Operative Treatments

Since the normal aging process and symptoms of disc degeneration are somewhat similar, it is not easy to distinguish the patient who need a surgical treatment and will benefit from it. Despite the fact that a minority of the people requiring spinal surgery, implications of such spinal disorders mentioned above as lumbar intervertebral disc disease and lumbar spondylosis cannot be overlooked in terms of economic and social distress (Oehme *et al.*, 2015).

Depending on the cause of the problem, there are several surgical treatment options available although not all patients can be neither managed nor addressed since there is not a single specific treatment that will solve all types of underlying problems. For example, microdiscectomy is one of the options, where a small portion of the disc is removed in order to decompress the affected nerve and decrease neurological symptoms. However, although 90% of the patients with sciatica have improvements, this approach does not address the underlying cause and may accelerate the degenerative process (Oehme *et al.*, 2015). In lumbar laminectomy, one of the options for lumbar spondylosis, de-roofing technique is used for the neural canal.

Most of the surgical operations aim decompression to relieve the symptoms. Decompressive procedures are reported to be preferable over the aggressive non-operative treatments in achieving improved functionality and symptoms (Weinstein, 2008). However, in some cases, back pain may persist and the decompression may lead to instability of the motion segments. Because of these reasons and other underlying conditions, many of the lumbar diseases are related to the instability of the motion segments and lumbar spine. Consequently, the fusion procedures are suggested where conservative and other surgical treatments fail. As the two or more adjacent bones of the

spine are united, the damaged disc is freed from the load and the compression is decreased, therefore the motion causing the pain is eliminated. Options of lumbar fusion include anterior or posterior approaches to the lumbar interbody fusion (ALIF and PLIF, respectively) and total disc replacement (TDR). Fusion procedures are among the most commonly performed procedures worldwide (Bono *et al.*, 2004). However, the effectiveness of the lumbar fusion is controversial. There are studies questioning the suitability of a surgical preference over cognitive-behavior therapy (Mirza & Deyo, 2007; Brox *et al.*, 2006) and also reports that speak against the effectiveness of a fusion procedure (Oehme *et al.*, 2015; Anderson *et al.*, 2015). On the other hand, there are reports on the benefits by managing the pain and improving the restricted mobility (Fairbank *et al.*, 2005; Ohtori *et al.*, 2011; Udby and Bech-Azeddine, 2015; Lamkli *et al.*, 2014). Therefore, fusion is only meaningful if those who can benefit from the procedure can be identified and operated (Willems, 2014).

The approach in the spinal fusion is to fuse and immobilize the unstable segment while maintaining the original disc height (Figure 1.6). Even if the intervertebral disc is not problematic, in such cases as scoliosis, the disc space including the endplates is cleared and with the help of intervertebral devices, the vertebral levels are fused. The immobilization is achieved by the insertion of a rigid construct such as plates, pedicle screws and rods, usually made of metal (Rutherford *et al.*, 2007). Plates or rods, depending on the type of the surgery, can be secured to the vertebral bodies using screws and enable fusion to occur. Some of these structures are presented in Figure 1.7.

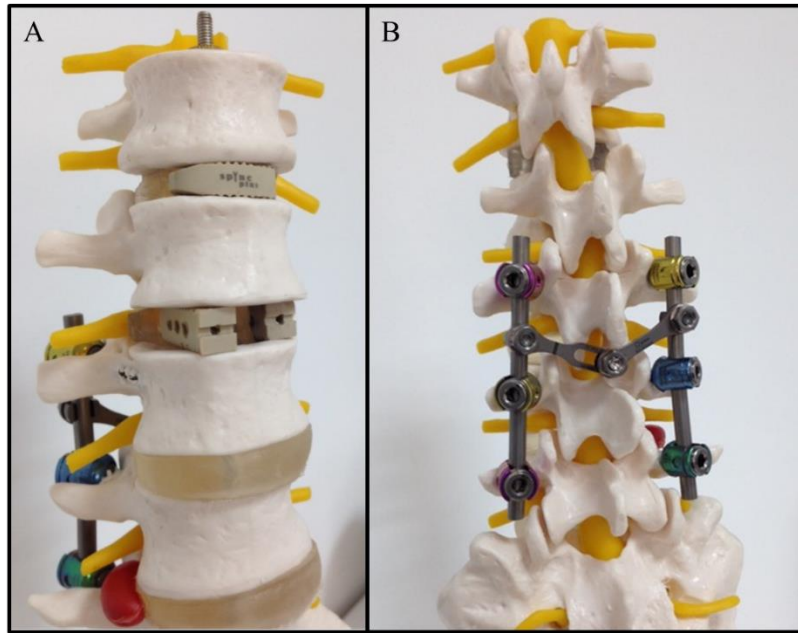


Figure 1.6 Model of some spinal fusion devices. (A) Spinal cage installation and (B) pedicle screw system. Intervertebral disc is cleared to open a space for the cage which is implanted and fixed between the two adjacent vertebra. The pedicle screw system is also used to fix the vertebral bodies. (Courtesy of Doratek Medical, Turkey)

An osteoconductive material or a scaffold such as an interbody cage with graft is also used to insert between the two vertebra. The most preferred osteoconductive material is autologous bone used with a graft, but to prevent the donor site morbidity, bone substitutes including calcium phosphates are preferred. In order to enhance the fusion rates, stem cells, demineralized bone matrix (DBM), ceramics and bone morphogenetic proteins (BMPs) are also used (Gupta *et al.*, 2015). One of the compounds used such as bone morphogenetic proteins (BMPs) are growth factors (Wozney, 2002). They constitute 0.1% (w/w) of all bone proteins (Gupta *et al.*, 2015) and by binding to the receptors on the surface of the osteogenic progenitor cells, they lead to calcification. After FDA approval, BMP-2 and BMP-7 were used (end of 2011) in 26.1% of lumbar fusion surgeries (Martin *et al.*, 2014). However, in order for BMPs to be effective, large amounts are needed and this increases the cost. After scientific reports critical of their use and

clinical concerns and risks, their use is decreased. A safer alternative to BMPs was considered to be the stem cells (Oehme *et al.*, 2015). Their potential to reverse or slow the degeneration of the disc, promotion of cartilage regeneration along with bone growth and fusion, low immunogenicity and potent antiinflammatory properties made them a viable alternative. However, the research on stem cells are still in progress while some state that stem cells make no difference (Ajiboye *et al.*, 2015; Kroeze *et al.*, 2014). However, in a recent research, mesenchymal stem cells (MSCs) were reported to increase patient safety and fusion rates up to 92 % (Kerr *et al.*, 2010). At present, there is not enough data to ensure long term durability and safety.

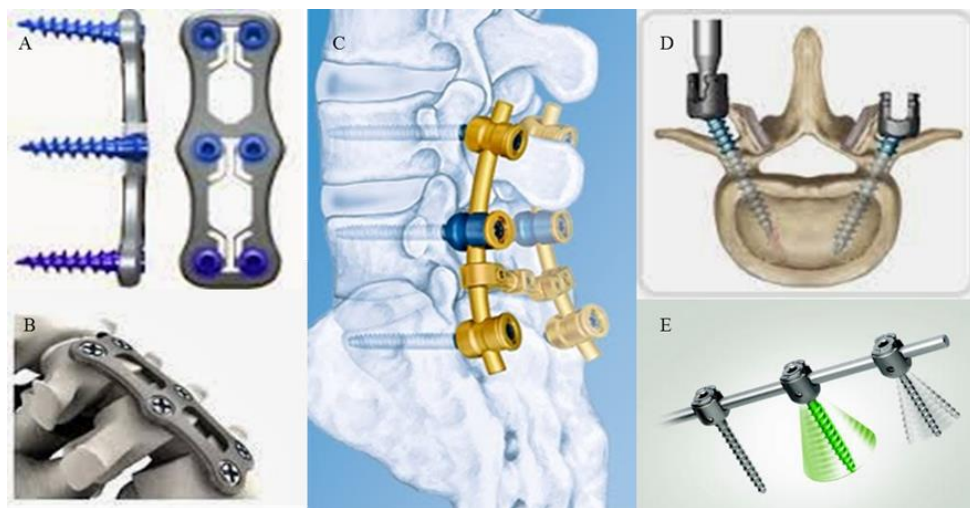


Figure 1.7 Some of the spinal fixation devices which includes plates, pedicle screw systems, rod and screw systems. (A)The Spider® Cervical plate (X-Spine Inc.), (B) Reflex® Hybrid Anterior Cervical Plate (Stryker Inc.), (C) The Click'X® Spine System (Synthes), (D) Denali® Degenerative (K2M Inc.), (E) The EXPEDIUM® Spine System (DePuy).

1.4. Lumbar Cages


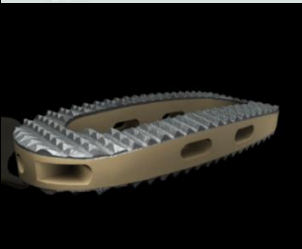
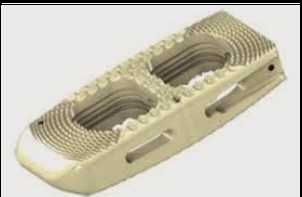


Apart from the devices such as rods, screws and plates, cages are one of the most commonly used medical devices in fusion surgeries. Spinal fusion cages, more specifically lumbar fusion cages, are developed to stabilize the lumbar vertebra and aimed to achieve pain management and stability in the spine (Kurtz *et al.*, 2007). These cages are used between the two vertebra to facilitate the fusion between them. The first metal cage designed was of stainless steel and proposed by Bagby (1988) to be used in a fusion technique to treat race horses with stenosis. Many cases of degenerative disc disease were then treated using spinal cages in clinical trials since 1991 and in the earlier studies, encouraging results with fusion rates as high as 90% were reported (Ray, 1997; Agazzi *et al.*, 1999) but they did not report long term follow-ups.

Other designs have porous structures, higher surface area and space allowing grafts to increase osteointegration lacked with steel implants (Wollowick & Sarwahi, 2015). Now it is known that both the design (Takeuchi *et al.*, 2015) and the material of the cages affect the fusion rates and the general outcome. Some commercially available designs of cages are illustrated in Table 1.2. Many of the designs, in general, have porous structure, fenestration patterns and threads to create space for the bone autografts and facilitate bone ingrowth. Controversy remains, however, as to the effectiveness of the cages since there are reports on cages subsiding, migrating or failing mechanically (Steffen *et al.*, 2000).

Table 1.2 Some selected commercially available fusion cages. Almost all are produced from titanium alloy and PEEK. The designs show variations based on the targeted problem.

Cage Name	Figure	Material	Description
BAK Interbody Fusion System (Zimmer Inc.)		Titanium alloy (Ti-6Al-4V)	Hollow, cylindrical, porous device to gather local autograft during the implantation
ADONIS®-TLIF (HumanTech)		Solid titanium	Curved shape for bilateral support and fenestrated structure for osteointegration
TM Ardis Interbody System (Zimmer Inc.)		Trabecular Metal	80% porous Trabecular Metal system, and high friction coefficient that prevents implant migration
Ray Threaded Fusion Cage (Surgical Dynamics Corp.)		Titanium alloy (Ti-6Al-4V)	Broad V-shaped threads and 70% fenestrations along the length of the cage to promote fusion
INTER FIX™ Threaded Fusion Device (Sofamor Danek Group)		Titanium alloy (Ti-6Al-4V)	Hollow, perforated, cylindrical cage with threads that allow integration
Varilift® (Wenzel Spine Inc.)		Titanium alloy (Ti-6Al-4V)	Expanding from cylindrical to wedge shape providing better fit and fenestrations for graft

Table 1.2 (Continued)

Cage Name	Figure	Material	Description
Opticage (iSpine Inc.)		Titanium	Expandable cage with large window for graft inclusion
VOX™ (Aurora Spine Inc.)		PEEK-OPTIMA & titanium coating	Porous titanium coating, resistance to creep and fatigue
CROSS-FUSE® (Pioneer)		PEEK-OPTIMA	Graft windows to increase fusion potential and teeth for better fixation
Endoskeleton® (Titan Spine)		PEEK & titanium coating	Curved shape to minimize the risk of subsidence, patterned surface to increase cell attachment
Cougar LS Lateral Cage System (DePuy Synthes)		Carbon Fiber Reinforced PEEK	Teeth along the surface to prevent migration of the cage

1.4.1. Materials Used in Lumbar Cages

The success of surgery in orthopedics depend, in addition to material design and properties, on the skills of the surgeon to fix parts of bones using rods, plates or screws and achieve unison between the implant material and the bone tissue. What also matters

though, is the metabolism and healing mechanisms of the bone. If these properties of the bone are better understood, then the clinical complications can be reduced (Buckwalter *et al.*, 1995). Therefore, researches are attempting to solve the problems with cages by developing materials that closely mimic the bone.

At the beginning, mechanical needs were taken into account and implants from mechanically strong materials such as titanium and stainless steel were designed (Weiner & Fraser, 1998). The problem with metals, however, was the high stiffness of a device made from them that did not match the properties of the bone, led to stress shielding, and therefore, inhibited bone growth. In addition, their radiopaqueness prevented prognostic assessment of the bone growth and healing.

In order to avoid the stress shielding observed with solid metals and also to better mimic the stiffness of the bone, tantalum cages with interconnected pores were developed. These cages were selected because of their low elastic modulus and a high friction coefficient which would help achieve better fixation of the implant (Hanc *et al.*, 2015). Tantalum cages are still in use as, for example, Trabecular Metal (Table 1.2).

Because of the excessive stiffness of the titanium cages, other materials like polymers were also investigated, one of them being poly(L-lactic acid) (PLLA). However, the results were not conclusive due to the limitations in bioabsorbability and the availability of only short term of follow up (6 months) (van Dijk *et al.*, 2002). Brenke *et al.* (2013) studied a cervical fusion cage made from a blend of polylactic acid and polyglycolic acid. They reported that 4 out of 33 patients presented cage dislocations although patients with cages that did not dislocate showed improvement with respect to pain. It was concluded that the present composition could not be used as a cage unless implant fixation is improved.

In addition to the lumbar cages, other biodegradable fusion devices were also tested. Yong *et al.* (2014) used poly(caprolactone) (PCL) scaffolds loaded with recombinant human bone morphogenetic protein-2 (rhBMP-2) as a fusion device in sheep spine and

concluded that it is a viable bone graft substitute. PCL was also used in combination with calcium phosphates (CaPs) instead of grafts in the fusion cages. β -Tricalcium phosphate (β -TCP, $\text{Ca}_3(\text{PO}_4)_2$), poly(ϵ -caprolactone) (PCL, $(\text{C}_6\text{H}_{10}\text{O}_2)_n$) and rhBMP-2 spinal cage were reported to create an appropriate environment for fusion and bone ingrowth (Abbah *et al.*, 2009).

The solubility of the calcium phosphates (CaPs) depend on their crystal structure and Ca:PO₄ ratios. CaPs with low calcium content are not very stable in wet environments, therefore, cannot be relied on for load-bearing applications. However, hydroxyapatite and other types of calcium phosphates are widely used within lumbar cages or as coating material in trying to imitate the bone composition and to accelerate the healing process and to increase the bone growth around the implant.

During the search for a better material for a cage, PEEK was found to match the mechanical properties of the bone better and to be easier to process than metals. Designs of the PEEK cages include both solid and porous structures. It was radiolucent and had good mechanical properties. In order to further enhance its quality, osteoinductive materials such as hydroxyapatite or BMPs were introduced in its structure (Roeder *et al.*, 2009). Currently, PEEK cages are one of the leading products investigated and used in the world (Toth *et al.*, 2005; Kasliwal & O'Toole, 2014; Voisin *et al.*, 2015).

1.4.2. Problems with Current Cage Materials

There is not a single material that is perfect for use as a cage material, because there are problems with each of them. Polymers, for example, can be easily processed but are not strong enough. Ceramics are osteoconductive but brittle and metals are durable but dense and difficult to process (Zhang *et al.*, 2007). Currently, fusion cages are commercially fabricated either from titanium alloys or polymers.

The main and the oldest problem with the metallic cages is a phenomenon called stress-shielding. As the mechanical stiffness is much higher than that of the bone, decreased mineralization of the bone, resorption and subsequent decrease in bone mineral density

(osteopenia) are observed in the long term (Lin & Wirtz, 2007). This is generally the case with all metallic implants as they carry the major portion of the load when implanted. In the case of devices such as plates, in order to avoid this problem, the metallic implant is removed after healing (Onodera & Funakoshi, 2015) However, since spinal cages are not to be retracted, their continued presence in the body is a problem in the long term. Titanium alloys, on the other hand, are prone to surface flaws which lead to fatigue failure.

Wang *et al.* (2015) reported the failure of a titanium mesh cage where the healing of the fusion area was not proper and the excessive stress was exerted on the cage. In a study where 26 patients were treated with trabecular metal cages for recurrent sciatica, it was observed that only 46 % of the patients reported good recovery during a 12 month follow up (Lequin *et al.*, 2014).

Other complications regarding cages, observed with the two most frequently used materials, PEEK and titanium, include low fusion rates, subsidence where the implant collapses, increase in the segmental lordosis (abnormal curvature of the motion segments), cage migration and mechanical failure of the implant. Nemoto *et al.*, (2014) compared the spinal fusion rates of titanium and PEEK cages with 48 patients and found that only 68% of the patients who received PEEK showed successful fusion in 12 months. They argue that in order to increase the low success rate of PEEK cages, biocompatibility, surface roughness and chemistry must be improved. In a case study by Stein *et al.* (2015) expendable PEEK cage was reported to fail and migrate towards the spinal canal, and no signs of fusion was observed and the patient had to undergo another surgery. Behrbalk *et al.* (2013) reported 5 cases of subsidence out of 25 in patients undergoing anterior lumbar interbody fusion using PEEK cage augmented with rhBMPs. Subsidence in the 17% of the PEEK cages was also reported by Flouzat-Lachaniette *et al.*, (2014).

Although PEEK is considered an appropriate material for fusion cages, there are limitations of the polymer. It is dense and bioinert (as is titanium), achieves ineffective fusion and have implant instability as the natural process do not allow it to fuse by

encapsulating the implant with a fibrous tissue (Roeder *et al.*, 2009). That is why almost all PEEK cages are supplemented with such osteoinductive materials as BMPs, bone material or grafts, or demineralized bone matrix to induce fusion. Even though not conclusive, the use of BMPs in spinal fusion have evidence of being involved in post-operative cancer diagnosis (Cahill *et al.*, 2015). Although tissue reactions to PEEK are scarce, they are reported to show allergic symptoms after surgery (Andres *et al.*, 2015). The inability of a cage to achieve fusion is another common complication. Schimmel *et al.* (2012) observed that 26 out of 96 patients who were treated with PEEK cages for degenerative disc disease had to undergo a secondary surgery due to pseudarthrosis where the two vertebra did not fuse. Still, in a clinical study where poly(L-lactide-co-D,L-lactide) (PDLLA) and PEEK cages were used, 50% of the patients with PDLLA cage showed improvement in pain scores as opposed to 71% of the patients with PEEK cages (Jiya *et al.*, 2010).

1.4.3. Poly(methylmethacrylate) (PMMA) and its use in Medical Devices

PMMA is a synthetic, amorphous, glassy, thermoplastic, hydrophobic polymer of methyl methacrylate (Figure 1.8). It has a high Elastic Modulus but does not shatter or elongate much upon failure. The glass transition temperature of PMMA is 100-130°C (Ali *et al.*, 2015). PMMA is relatively easy to process, has low cost and better mechanical properties than most polymers. It is tolerated by human tissues and does not cause necrosis or inflammatory reactions (Moreno *et al.*, 2015).

Initially, it was used as a fixation device and currently it is more used as a filler in the form of bone cement, a mixture used to stabilize total hip implants, among others. Farrokhi *et al.* (2010) in a pilot study, proposed an acrylic cage with high stiffness and less subsidence than grafts. In a follow up study in 2015, they compared a PEEK cage with an acrylic cage in a clinical study with 64 patients and found that acrylic cages could be a better alternative to bone grafts and other cages due to their good clinical (with 3% higher fusion rate than PEEK) and radiological results. There are other reports on the use of PMMA as a fusion cage with minimal complication rates (5% in 249 patients,

Hamburger *et al.*, 2001) and high fusion rates (100% after 12 month examination, Chen *et al.*, 2005). Also, the low cost and short preparation time of PMMA as well as the similar or superior mechanical properties than PEEK are important advantages of PMMA (Brenke *et al.*, 2014).

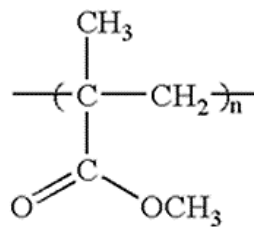


Figure 1.8 Chemical structure of poly(methylmethacrylate) (PMMA).

Although the increasing temperature due to the exothermic polymerization reaction during the setting of the cement in the defective site may lead to thermal damage, PMMA is still used as the most common cement material (Boger *et al.*, 2009). It is often used with supplementary materials to enhance the bioactivity, osteoconductivity and the mechanical properties. Arabmotlagh *et al.* (2014) conducted an *in vivo* research with sheep where PMMA was used in combination with up to 30 % hydroxyapatite (HAp) as a filler for the osteoporotic vertebral fractures and observed that the fatigue failure rate was lessened in comparison to plain PMMA. Moreover, Liu *et al.* (2015) studied the *in vitro* effects of PMMA with HAp mixed with BMP-2 and showed that this material can be used as a bioactive material in load bearing applications.

1.5. Aim and Novelty of the Study

There is not a single material that can be safely and successfully used in a fusion cage and there are many problems mentioned before, regarding all of them.

Poly(methylmethacrylate) (PMMA) is one of the most used material in orthopedic devices and there are several reports concerning the improvements of material mechanical properties in matching that of the application site and the responses of the bone tissue to the implant. In fusion cages, crucial aspects are the mechanical properties of the cage matching that of the vertebra so that stress shielding can be avoided, and appropriate fusion. The aim of this study was to develop a polymeric material with sufficient mechanical properties to meet the mechanical requirements of the spine, and with enhanced osteoconductive properties to increase bone ingrowth to be used as a fusion cage. In order to develop such a structure, varying amounts of PMMA and hydroxyapatite (HAp) were brought together by hot melt extrusion method and molded by injection. Mechanical characterizations and *in vitro* studies were conducted using these materials.

There are reports on the use of PMMA as fusion cages and as void fillers, and studies to enhance the tissue response to PMMA by adding supplementary materials. However, there is no such report where PMMA and HAp are used in combination as a fusion cage. The novelty of this study, therefore, is to produce such a composite with an appropriate PMMA:HAp ratio by compounding PMMA and HAp with hot melt extrusion and by injection molding the material so that the mechanical and osteoconductive properties are appropriate for a specific load bearing application.

CHAPTER 2

MATERIALS AND METHODS

2.1. Materials

Poly(methylmethacrylate) (PMMA, average $M_w \sim 996,000$ by GPC, crystalline), bovine serum albumin (BSA), Alizarin Red S and ascorbic acid were purchased from Sigma-Aldrich (Germany). Hydroxyapatite (HAp, $\geq 90\%$ as $\text{Ca}_3(\text{PO}_4)_2$), was purchased from Fluka (Germany). Alexa Fluor® 488 FITC-conjugated phalloidin was purchased from Life Technologies, Thermo Scientific (USA) and DRAQ5 from Abcam (UK). McCoy's 5A Medium, penicillin-streptomycin (10,000 units/mL each) and L-glutamine (20 mM 0.85 % NaCl solution) were bought from Lonza (Belgium). Dulbecco's Modified Eagle Medium (DMEM) high glucose without phenol red was obtained from Biochrom (Germany), Fetal Bovine Serum (FBS) and trypsin (0.25 %) – EDTA (0.02 %) in HBSS from Biowest (USA), Amphotericin B (250 $\mu\text{g}/\text{mL}$) from HyClone, Thermo Scientific (USA), and Alamar Blue from Invitrogen Inc. (USA). Dimethyl sulfoxide (DMSO) was obtained from Fisher Scientific (USA) and Triton-X 100 was from AppliChem (USA).

2.2. Methods

2.2.1. Preparation of PMMA-HAp Composites

2.2.1.1. Compounding and Extrusion of PMMA and HAp

0, 10, 20, 30 and 40 (w/w) PMMA-HAp mixtures were prepared using a compounder-extruder (Figure 2.1A) (Haake MiniLab II, Thermo Scientific, Germany). Each batch of 2 g, constituting the total of approximately 4 g within the device, were compounded for

at least 30 min under 10-20 rpm rotation speed, 60-100 N.cm torque and 80-100 bar pressure. Working temperature was optimized as 220-230°C in order to ensure the optimum processing conditions with different HAp contents. The composite was extruded as fibers using a 1 mm orifice, and pelletized into 1-2 mm pieces.

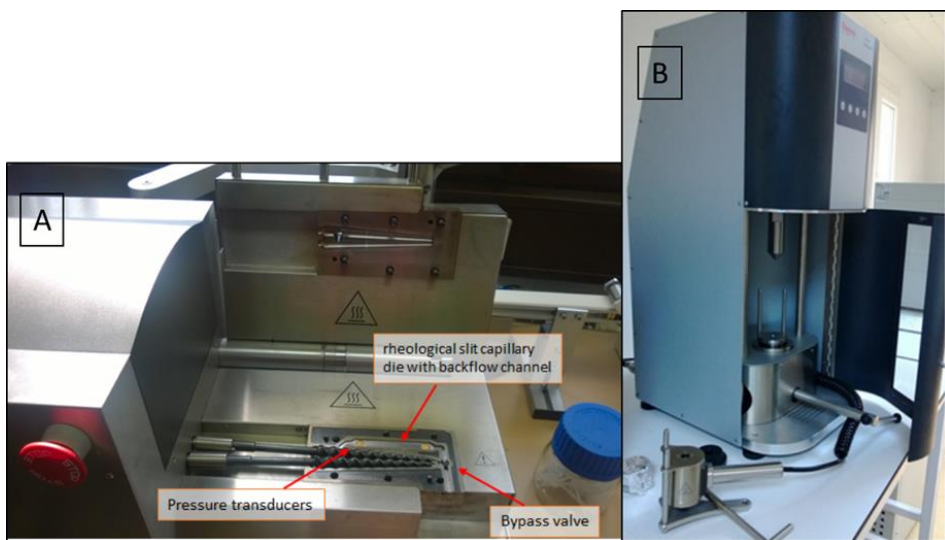


Figure 2.1 The two devices used to produce used to produce pure PMMA and PMMA-HAp composite plates. (A) Compounder-extruder and (B) injection molder.

2.2.1.2. Injection Molding of the Composites

PMMA-HAp pieces were loaded into the cylinder of the injection molder (Figure 2.1B) (Haake MiniJet, Thermo Scientific, Germany) at $250 \pm 5^\circ\text{C}$, and the molten mixture was injected into the mold at 100°C under 1000 bar injection pressure for 10 s and 400 bar post-pressure for 10 s. The molds were dog bone shaped, which were also suitable for ISO 527 mechanical testing and bar shaped with the dimensions of 80 mm x 1 mm x 10 mm (Figure 2.2). Bar shaped plates were also cut into 1 cm^2 samples for use in the *in vitro* studies.

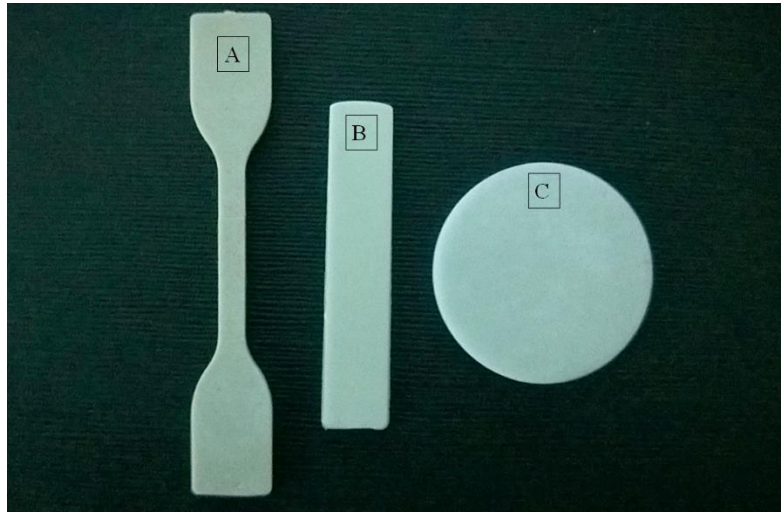


Figure 2.2 Injection molded PMMA-HAp composite samples. (A) Dog-bone shaped sample was used in the tensile tests, and (B) bar shaped samples were used for the compression and *in vitro* tests. (C) Disc samples were not used in this study.

2.2.2. Characterization of the PMMA-HAp Composites

2.2.2.1. MicroCT imaging

Dry samples of pure PMMA and PMMA-HAp composite plates were scanned by X-ray using a microcomputed tomography system (SkyScan 1172, Bruker, Belgium). The dimensions of the specimens were 10 mm x 10 mm x 1 mm and they were scanned for 360°. The organic material (PMMA) is translucent meaning it is expected to let the beam through and minerals (HAp) to hold the X-ray so that they are observed as white spots.

2.2.2.2. Mechanical Testing

All mechanical tests were conducted on a Shimadzu AGS-X universal test machine (Japan) at room temperature. Four samples of each composition in the shape of dog bone were used for tensile testing (Figure 2.3). Ends of the samples were stabilized with the clamps with a gauge length of 30 mm. Crosshead speed of the load cells was 1 mm/min. Stress (σ) and strain of the samples were calculated from the equation (I) and (II).

$$\sigma = \frac{F}{A} \quad \text{and} \quad \varepsilon = \frac{\Delta L}{l} \quad (I) \text{ and } (II)$$

where F was the force (N) in the direction of the pull, A was the cross sectional area of the sample (mm^2), ΔL was the difference in sample length (mm) and l was the initial sample length (mm). Another property measured was the Elastic Modulus (E):

$$E = \frac{\sigma}{\varepsilon} = \frac{F}{\Delta L} \times \frac{l}{A} \quad (III)$$

where E was the Elastic Modulus (MPa), σ was the stress (MPa), ε was the strain. The ultimate tensile strength (UTS) is the maximum stress observed during the test and is calculated by dividing the maximum force the sample endured during the test over cross sectional area (Equation IV).

$$UTS = \frac{F_{max}}{A} \quad (IV)$$

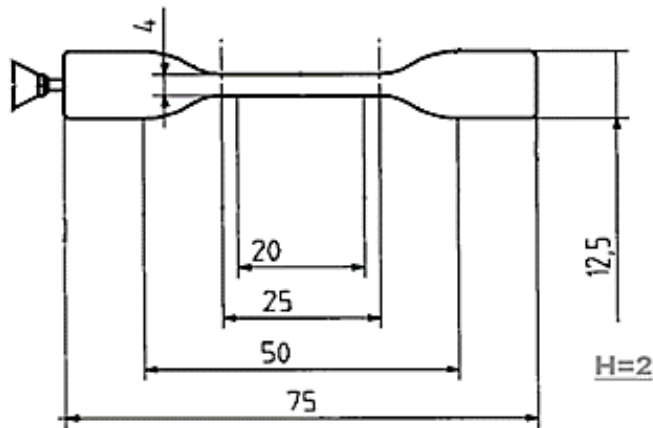


Figure 2.3 Dimensions of a dog bone sample suitable for testing according to ISO 527 standard for tensile test.

Bar shaped plates (80 mm x1 mm x10 mm) of each composition were also tested under compressive loads (n=3). In order for the samples not to bend, a custom support rig was used to stabilize the samples in upright position exposing an unsupported section of 10 mm. The crosshead speed of the tests was 1.5 mm/min. As explained in the ASTM D 695 Standard Test Method for Compressive Properties of Rigid Plastics, the elastic modulus in compression was calculated by drawing a tangent to the initial linear curve, and dividing the compressive stress at any point on this line to the corresponding strain (Figure 2.4). The result of modulus was expressed in GPa. The compressive strength was calculated by dividing the maximum load carried by the initial cross sectional area of the plate. The results were expressed in MPa.

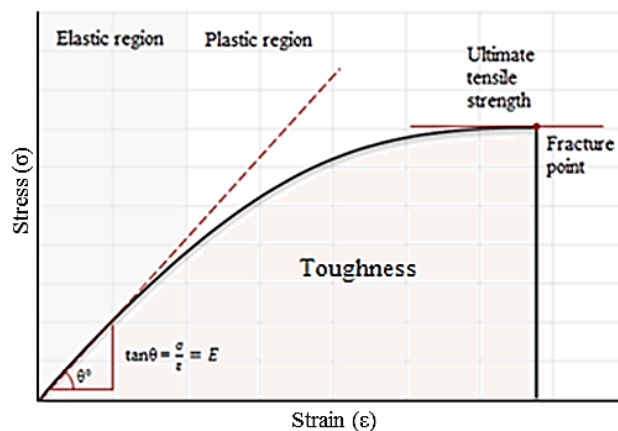


Figure 2.4 Characteristic stress-strain curve of pure PMMA obtained in this study. E is the elastic modulus calculated as the ratio of stress (σ) to strain (ϵ) at the elastic region.

2.2.2.3. Scanning Electron Microscopy (SEM) and Energy Dispersed X-Ray (EDX) Analysis

SEM and EDX (energy dispersed X-ray) analysis of dry samples were coated with Au-Pd under vacuum using a sputter coater and examined under high vacuum with a scanning

electron microscope (FEI, Quanta 400 FEG, USA). Images with x250 and x5000 magnification were recorded.

2.2.2.4. Surface Profilometry

Optical surface profilometers measure the height variations on a surface using wave properties of the light. The path of the light reflected from the test surface is compared with that of a reference surface and a profile of the surface is obtained. The characterization of the surfaces of pure PMMA and PMMA-HAp composite plates were constructed using an optical surface profilometer (Zygo, NewView™ 3D Optical Surface Profiler, USA). The surfaces of the dry samples were analyzed with respect to topography of either area or evaluation length as a linear path along the surface and expressed also as histograms. Root square mean (rms) values of the roughness of the surface areas obtained are calculated by the profilometer by using the following formula:

$$rms = \sqrt{\frac{1}{L} \int_0^L z^2(x) dx} \quad (V)$$

where L: evaluation length, z(x): surface height function.

2.2.2.5. Contact Angle

Water contact angles of dry of pure PMMA and PMMA-HAp composite samples were determined using a goniometer (Attension, Biolin Scientific, Sweden). 4 samples of each composition were studied. For each of the plates, 7 μL of dH₂O was placed onto the sample surface as a sessile drop and the contact angles recorded from 3 points on the test sample were expressed as average of the measurements. The wettability assessment of the surfaces by contact angle measurement is depicted in Figure 2.5.

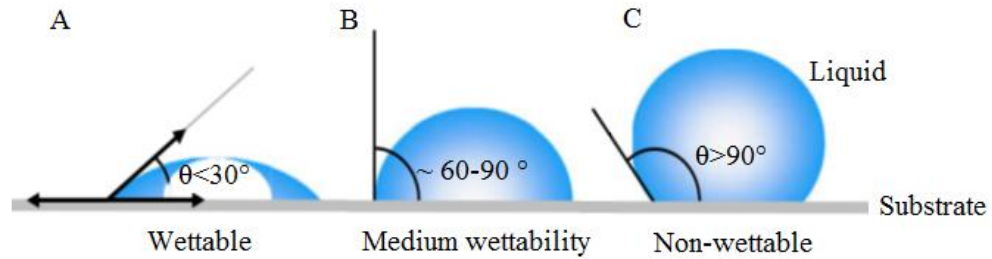


Figure 2.5 The contact angle of a liquid with a substrate gives the wettability of the surface. If the angle is (A) below 30° , the material is said to be wettable, and if (C) above 90° , non-wettable. Adapted from Yuan & Lee (2013).

2.2.3. *In vitro* Studies

2.2.3.1. Isolation of Human Osteoblast-like (HOB) Cells

The human osteoblast-like cells used in this study were isolated by Menekşe ERMİŞ ŞEN and Esen SAYIN at BIOMATEN (METU, Turkey). Ethical committee authorizations were obtained from Gülhane Medical Military Academy (GATA) and METU. The cells were isolated from bone fragments obtained during surgery. These fragments were washed with PBS (phosphate buffer saline) and DMEM (Dulbecco's Modified Eagle Medium) without serum. After cutting into small pieces, the fragments were transferred into tissue culture flasks and supplemented with McCoy's 5A growth medium. The flasks were not disturbed for the first 7 days; later the medium was refreshed once every 4 days. As the migrating cells reached 90% confluence, they were trypsinized and passaged.

2.2.3.2. HOB Cell Culture

The human osteoblast cells (HOB) were cultured in sterile tissue culture polystyrene (TCPS) flasks in a growth medium containing McCoy's 5A supplemented with total 10 % fetal bovine serum (FBS), 1% penicillin-streptomycin (final concentrations 10,000

units/mL each), 0.5 % L-glutamine (20 mM in 0.85 % NaCl solution), 0.03 % ascorbic acid, and 0.1 % amphotericin B (250 mg/mL). Cells were cultured at 37°C in 5% CO₂ incubator, and the medium was refreshed every other day. When cells reached confluence, the medium was discarded, cells were washed with PBS and trypsin solution was added (diluted to 0.05% from a 0.25% stock in PBS) at 37°C for 5 min. Detached cells were collected by centrifugation at 5,000 rpm for 5 min and suspended in supplemented McCoy's 5A full medium (Lonza, Belgium).

2.2.3.3. Cell Seeding on PMMA-HAp Composites

The plates were immersed in 70 % EtOH for 30 min for sterilization, and then washed with sterile dH₂O and left to dry in air. Following sterilization, scaffolds were transferred into 24 well tissue culture plates. Cells were collected as described in the previous section and seeded onto 1 cm² square test plates at a density of 10⁴ cells/cm². The cell seeded plates were incubated at 37°C in 5% CO₂ incubator for 1 h for the cells to attach. Then, 1 mL of medium was added to each well, incubation was continued and medium was refreshed every other day.

2.2.3.4. Cell Viability Assay

Alamar Blue assay was conducted to study the attachment and proliferation of the HOB cells seeded on pure PMMA and PMMA-HAp composite test plates. On Days 1, 3, 7 and 14, medium was discarded and plates were washed twice with PBS. Plates were incubated for 2.5 h at 37°C and 5% CO₂ with 10% Alamar Blue solution (v/v) in DMEM high colorless medium supplemented with 1% penicillin-streptomycin (10,000 units/mL-each), and 0.5% L-glutamine (20 mM in 0.85 % NaCl solution). At the end of incubation, 200 µL of solution was transferred into 96 well plates and absorbance values were measured at 570 nm (λ_1) and 595 nm (λ_2) with a UV/Vis microplate spectrophotometer (Multiskan Spectrum, Thermo Scientific, USA). The reduction of the resazurin sodium salt in the dye to strongly fluorescent resorufin sodium salt was calculated using the following equation:

$$\text{Reduction \%} = \frac{((\epsilon_{ox})_{\lambda_2} \times A_{\lambda_1}) - ((\epsilon_{ox})_{\lambda_1} \times A_{\lambda_2})}{((\epsilon_{red})_{\lambda_1} \times A'_{\lambda_2}) - ((\epsilon_{red})_{\lambda_2} \times A'_{\lambda_1})} \times 100 \quad (VI)$$

where A_{λ_1} =Absorbance of test well at λ_1 , A_{λ_2} = Absorbance of test well at λ_2 , A'_{λ_1} =Absorbance of negative control well (blank) at λ_1 , A'_{λ_2} = Absorbance of negative control well at λ_2 . The extinction coefficients for the two forms of the dye at different wavelengths are presented below:

$\lambda_1 = 570 \text{ nm}$	$\lambda_2 = 595 \text{ nm}$
$(\epsilon_{ox})_{\lambda_1} = 80.586$	$(\epsilon_{red})_{\lambda_1} = 155.677$
$(\epsilon_{ox})_{\lambda_2} = 117.216$	$(\epsilon_{red})_{\lambda_2} = 14.652$

A calibration curve was prepared using the same procedure with known number of cells to convert the absorbance values into cell numbers (Appendix A). The assay was conducted in triplicates for each composition. Cells on TCPS (tissue culture polystyrene) were used as the control group.

2.2.3.5. Microscopic Characterization of HOB Cells

2.2.3.5.1. Confocal Laser Scanning Microscopy

Morphology and the organization of the cytoskeleton of the HOB cells were studied using confocal laser scanning microscope (Leica DM2500, Germany). HOB cells seeded on the plates of pure PMMA and PMMA-HAp composites were washed twice with PBS on Days 3, 7 and 14, and fixed with 4% paraformaldehyde for 15 min at room temperature. Prior to staining, cells were permeabilized with Triton X-100 (0.1% v/v in 10 mM Tris-HCl buffer) for 5 min, and washed with PBS to remove any residues. Each plate was treated with 1 % BSA and incubated for 30 min at 37°C. After that, seeded plates were incubated with FITC-labeled Phalloidin (0.5 $\mu\text{g/mL}$ in 0.1% BSA in PBS) for 1 h at 37°C to stain the cytoskeleton, washed with PBS, and then treated with DRAQ-5 dye for 15

min at room temperature to stain the nucleus. All plates were stored in PBS at 4°C until analysis.

2.2.3.5.2. Scanning Electron Microscopy Analysis

Cell culture media were removed from the plates and washed with PBS. Cells are fixed with 4% PFA (paraformaldehyde) for 15 min at room temperature on Days 3, 7 and 14. Cultured plates were incubated in 1% osmium tetroxide (Sigma Aldrich, Germany) solution for 1 h at room temperature. After washing thoroughly with dH₂O, plates were dried with a graded series of ethanol 50, 70 and 100% EtOH for 5 min each, respectively. Samples were then freeze dried for 2 h and stored in a desiccator until examination as explained in section 2.2.2.3.

2.2.3.6. Alizarin Red Staining

After 7 days in culture, cells on the plates were fixed in 4% PFA in PBS for 15 min at room temperature after removing the media and washing with PBS. Following the fixation, plates were washed with distilled water (dH₂O) to remove any PFA or salt residues. Cells on the plates were dyed with 1% Alizarin Red S (w/v, pH: 4.5) (Sigma Aldrich, Germany) for 30 min at room temperature.

2.2.4. Statistical Analysis

The quantitative data in this study are expressed as mean \pm standard deviations with $n \geq 2$ unless otherwise stated. Statistical analysis was performed by one-way ANOVA (analysis of variance) test followed by Tukey's test using SPSS 20.0. *p*-values less than 0.05 are considered statistically significant.

CHAPTER 3

RESULTS AND DISCUSSION

3.1. Preparation and Characterization of PMMA-HAp Composite Plates

In this study, the goal was to blend HAp with PMMA at such a level that the inorganic particles were distributed throughout the polymer and were also present on the surface of the sample to serve as cell attachment sites. Additionally, when the HAp on the surface was hydrolyzed, the plate was expected to become porous enabling the cells in the neighboring tissue to grow into the plate and lead to better integration than a non-porous, smooth, non-ionic PMMA plate would (Zhao *et al.*, 2013). At this point, a different kind of CaP could also be used instead of HAp. For example, tricalcium phosphate (TCP) is also osteoconductive and would help to improve the mechanical properties. However, the degradation rate is much faster than that of HAp which would lead to a porous structure sooner than needed. HAp was chosen for use in this study so that cells would find attachment sites as the healing process continues and that the composition would be as close to that of the natural bone as possible.

3.1.1. Distribution of HAp Particles in PMMA

Hot extrusion method was used in preparing PMMA plates to properly compound the PMMA and HAp particles. One method to show the distribution of HAp particles within PMMA is the microcomputed tomography (microCT). CT imaging is a widely used method in *in vivo* 3D imaging, and due to the ability to obtain high resolution, deep penetration of X-rays and high magnification, microCT provides a more suitable

evaluation method for *in vitro* research and biomaterial characterization (Savatier *et al.* 2014).

The results of the microCT imaging of the PMMA plates carrying varying amounts of HAp are presented in Figure 3.1. Since the HAp particles are opaque to X-ray because of the presence of high atomic number elements such as calcium and phosphorous, HAp particles are observed as white spots within the radiotransparent PMMA structure. As the HAp content in the mixture is increased, the particles in the image also gradually increased. The distribution of HAp particles within the plate was satisfactory also showing that the HAp did not aggregate to lead an uneven mechanical properties.

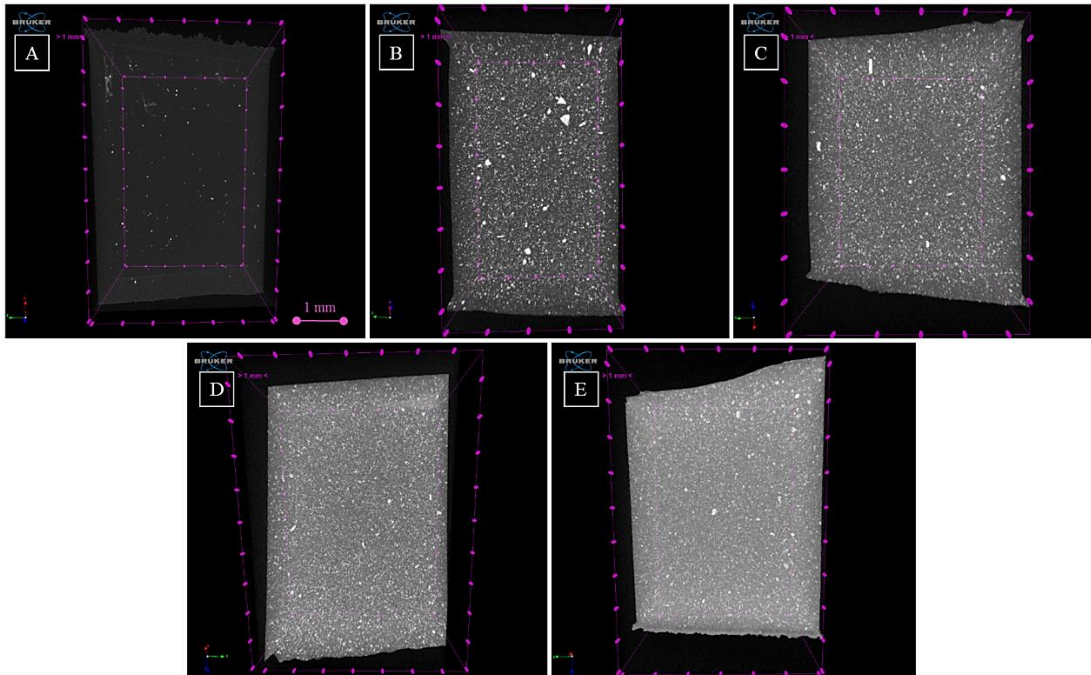


Figure 3.1 MicroCT images of PMMA samples carrying varying amounts of HAp. (A) Pure PMMA plate, HAp (% w/w): (B) 10, (C) 20 (D) 30, (E) 40. The opaque spots could be observed to increase with an increase in the HAp content. The control sample, pure PMMA does not show any HAp.

3.1.2. Mechanical Properties

In general, any kind of load bearing bone implant such as a spinal fusion cage, should match the mechanical properties of the application site. Therefore, tensile and compressive properties of the pure PMMA and PMMA-HAp composites were determined in order to compare them with the properties of the bone and commercially available products. Compressive and tensile properties of the materials in this study and some properties of bone and PEEK are presented in Table 3.1.

Polymers change their mechanical behavior depending also on the temperature. As the temperature exceeds glass transition temperature (T_g) of the polymer, the polymer becomes relatively less brittle and more rubber-like. Since the T_g of PMMA is much higher than the body temperature and the room temperature at which the experiments were conducted, no difference in the test results were expected.

When mechanically testing a specimen and comparing it to the natural bone, it should be taken into consideration that the bone is an anisotropic material and give different results longitudinal and transverse directions. The specimens in this study were treated as isotropic in the direction of the flow of the molten polymer during the injection molding process. The resulting effects of the processing were observed as streaks on the surface as was presented in Figure 3.5 in the section 3.1.3.

Table 3.1 Summary of the some tensile and compressive properties of the materials used in this study, PEEK and bone.

	Tension				Compression			Ref.
	UTS (MPa)	ϵ (%)	(GPa)	T_t (J)	Compressive Strength (MPa)	E_c (MPa)	T_c (J)	
PMMA	70.80	6.62	2.08	0.85	72.24	349.24	0.83	Present study
10 % PMMA-HAp	65.44	5.76	2.15	0.67	96.12	411.26	2.37	
20 % PMMA-HAp	68.23	4.66	2.46	0.48	105.52	517.79	1.42	
30 % PMMA-HAp	68.57	2.96	3.02	0.24	98.83	473.01	1.31	
40 % PMMA-HAp	66.50	2.17	3.92	0.18	103.58	562.26	2.37	
PMMA	48.3-72.4	2.0-5.5	2.24-3.24					Callister, (2007)
PEEK	103		3.58-4.00					Harper, (2000)
Cortical bone	50-151		12-18			130-180		Wagoner Johnson & Herschler (2011)
Trabecular Bone (wet)	1.17		0.06-0.80		5	50		Goldstein <i>et al.</i> (1991)
Lumbar Vertebrae (wet)	3.70		0.34					Saha & Pal (1984)

ϵ : strain in tension, UTS: ultimate tensile strength, E_t : elastic modulus in tension, E_c : elastic modulus in compression, T_t : tensile toughness, T_c : compression toughness.

3.1.2.1. Tensile Properties

Characteristic stress-strain curves of each composition and pure PMMA are presented in Figure 3.2. Stress (σ) is the force exerted on the area (cross section) of the tested sample, the highest values of which is the ultimate tensile strength (UTS). There was no significant difference ($p>0.05$) between none of the samples with respect to each other and UTS varied between 65.4-70.8 MPa. On the other hand, as the sample is subjected to

the tensile forces, it elongates even though a very small amount compared to most polymers. As the hydroxyapatite content increased, elongation under tensile stress responded accordingly.

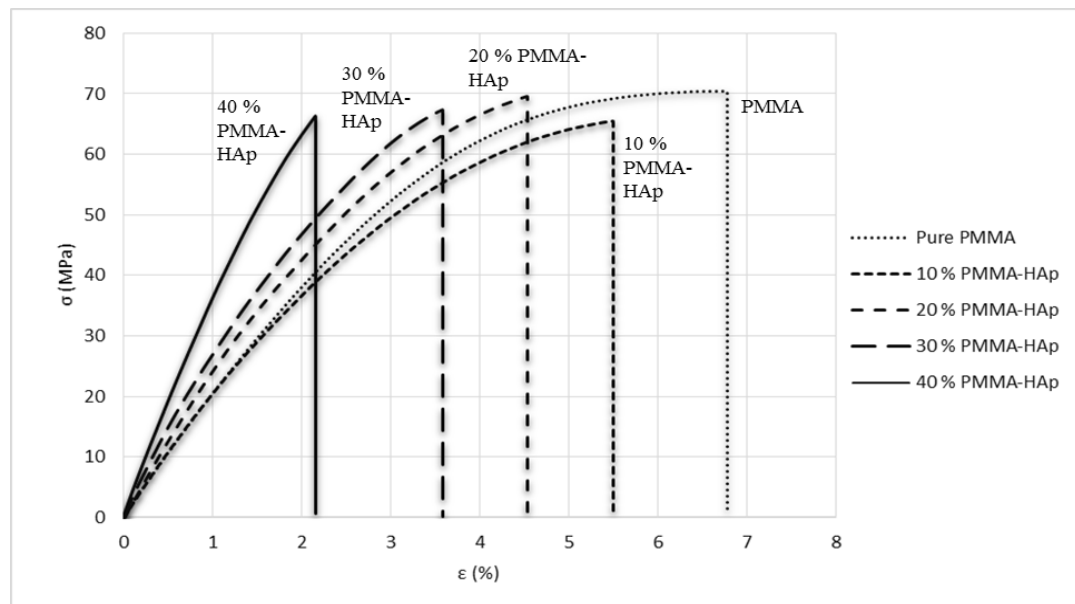


Figure 3.2 Characteristic stress-strain curves for pure PMMA and PMMA-HAp composites under tension. At the elastic region, the initial slope of the stress-strain curve gives the elastic modulus (Young's modulus, E), and the maximum value of the stress divided by the corresponding strain gives ultimate tensile strength (UTS). The tests were carried out at room temperature and the crosshead speed was 1 mm/min.

The maximum elongation at the break kept a steady decrease from 6.62% with pure PMMA to 2.17% with 40% (w/w) HAp content in PMMA. This probably is because the higher the mineral content; the interaction between the polymer chains is decreased, and therefore, they fail upon the application of tension. This decrease in strain, as it can be seen in Figure 3.2, means that the pure PMMA that had a ductile behavior, became stiffer and more brittle with increasing content of HAp in it. If a material is stiffer, the elastic

modulus is higher and deformation is more difficult, as is the case with PMMA having increasing amounts of HAp.

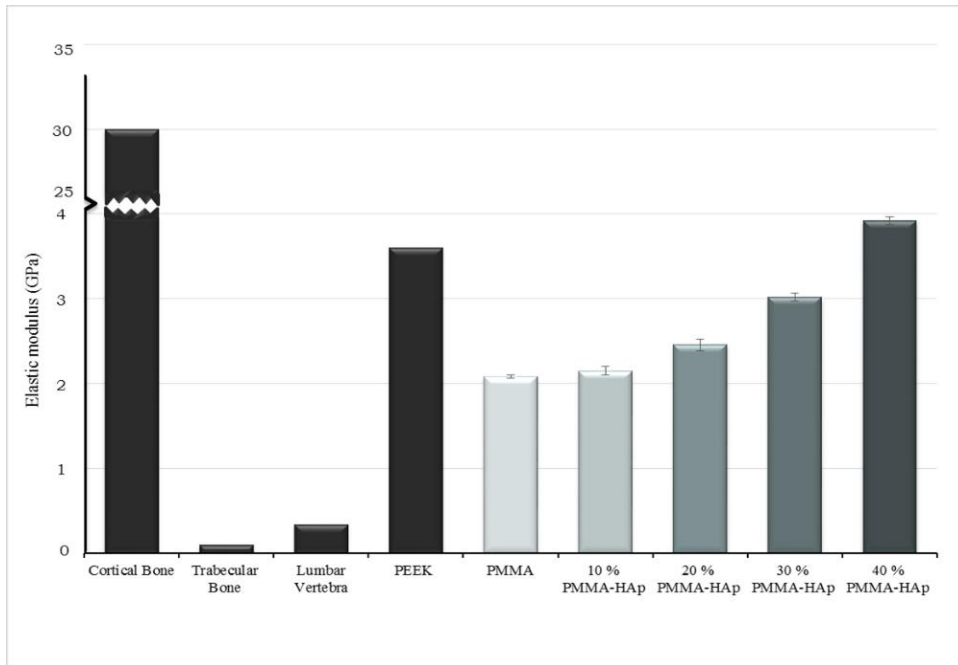


Figure 3.3 Elastic moduli of the pure PMMA and PMMA-HAp composites, cortical and trabecular bones (Wagoner Johnson & Herschler, 2011), lumbar vertebra (Saha & Pal, 1984), and PEEK (Harper, 2000).

Elastic moduli of the pure PMMA and PMMA-HAp composites, as well as that of bone and PEEK are presented in Figure 3.3 and Table 3.1. Cortical bone is by far the stiffest material of all whereas the trabecular bone and the lumbar vertebra are the softest of all. Pure PMMA is seen to have an elastic modulus of 2.08 GPa which is almost half that of PEEK. Other compositions of PMMA-HAp have moduli increasing almost linearly with the content of the hydroxyapatite in the composition. Modulus of the 40% HAp (w/w)

loaded PMMA exceeded that of PEEK which the most commonly used material in commercial fusion cages.

All the other blends (HAp < 40%, w/w) had elastic modulus lower than that of PEEK and the cortical bone, but above the trabecular and lumbar bone. Although the geometric shape of the implant and other mechanical properties such as stiffness should be taken into consideration when assessing the mechanical characteristics of the material, the stress shielding is still a problem commonly observed with such materials used in fusion cages as titanium and PEEK that have mechanical properties much higher than that of the natural bone. As such the stiffness of the blends with 30% (w/w) or lesser are more suitable for use as fusion cages since stress shielding will not be a problem (Kurtz & Devine, 2007; Uthoff *et al.*, 2006).

3.1.2.2. Compressive Properties

The data for elastic modulus under compression and compressive strength are given in Figure 3.4. Elastic moduli of the plates showed an increase in compression, with HAp composition up to 20%. Compressive strength also increased up to 20% (w/w) HAp, and then the rate of increase leveled off. The overall compressive strength was lower than that of cortical bone and PEEK, which suggests that PMMA-HAp composites were suitable for use as a bone implant as the strength should not exceed that of the cortical bone.

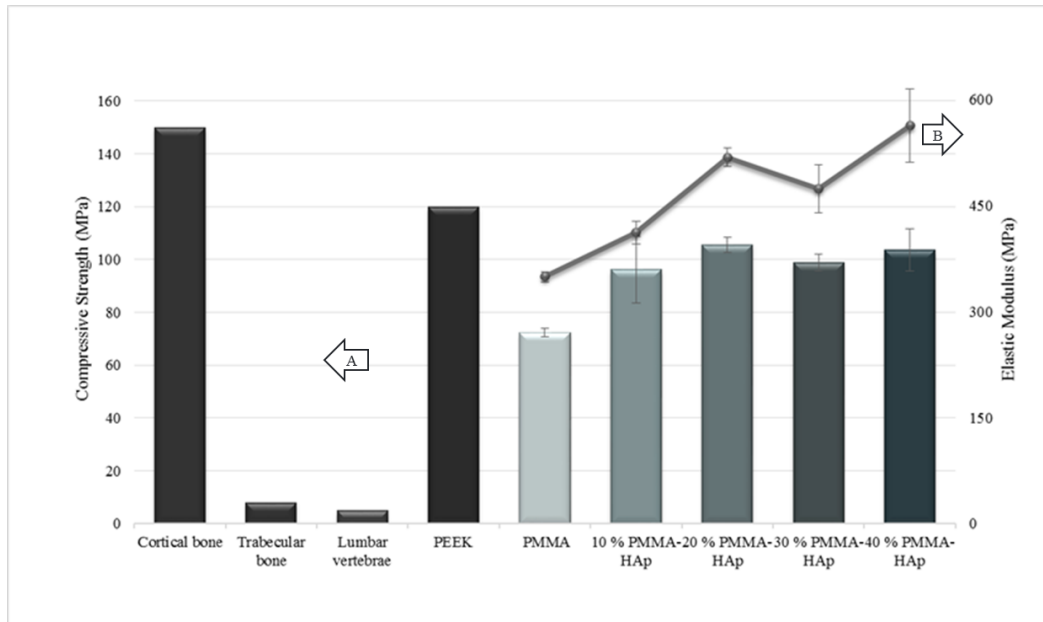


Figure 3.4 Compressive properties of some bone samples and cage materials. The samples tested in the study were pure PMMA and PMMA-HAp composites. (A) Compressive strength, (B) elastic modulus.

In some of the studies regarding the mechanical properties of composites of PMMA and HAp, compressive strength was found to decrease or remain unchanged with HAp content increase. In two studies, after 2.5% (w/w) HAp inclusion, compressive yield strength were reported to decrease (Zebarjad, 2011, and Vallo *et al.*, 1999). Also, in another study by Kang *et al.* (2012), compressive strength, as well as the UTS, of the PMMA-HAp composite decreased when HAp was introduced and also when its amount increased from 0 to 40% (w/w) HAp content. In all these studies, the decrease of the compressive properties was generally attributed to the insufficient adhesion of the ceramic with the polymeric matrix. The reason, therefore, for the improvement of the compressive properties of the composite plates in the present study may be a more effective interaction provided by the hot melt extrusion followed by a cycling process used in our protocol with the compounder-extruder.

In the light of the mechanical data, it can be concluded that the mechanical properties of the PMMA is enhanced by the incorporation of HAp. This provides a material better suited to the requirements of the spinal loads which especially is very important in compression. On the other hand, the strength should not significantly exceed that of the bone, as in the case of metallic bone implants preventing the slowing down of the healing process due to the stress shielding (Sumner *et al.*, 1998).

3.1.3. Scanning Electron Microscopy Analysis

Figure 3.5 shows the scanning electron microscopy (SEM) images of the pure PMMA and PMMA-HAp composite plates. Results of the pure PMMA qualitatively show the smoothest surface. Roughness of the surface is observed to increase with the relative HAp content. 40 % (w/w) PMMA-HAp composite plate had the roughest surface of all. What is more is that the surfaces showed streaks, likely to be the result of the processing technique which includes high pressure compression forcing molten polymer to fill the mold in one direction during the injection molding step. These streaks were expected to influence cell alignment when seeded on these plates and were treated as an isotropy, especially when mechanical tests were performed.

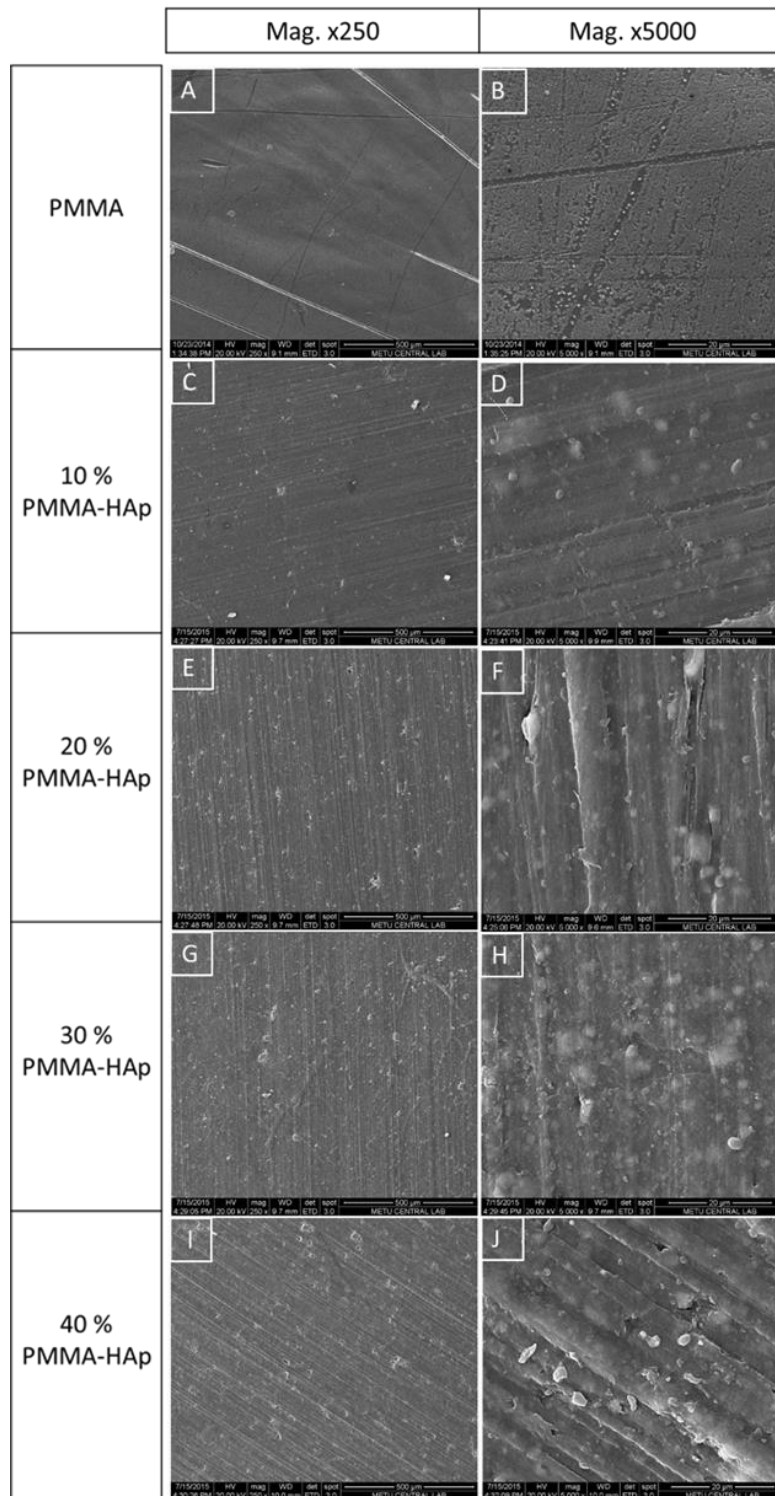


Figure 3.5 SEM images of PMMA and PMMA-HAp plates. Pure PMMA shows the smoothest surface and as the HAp content increases, the roughness of the surfaces increases as well. (A,C,E,G,I) Mag. x250 and (B,D,F,H,J) x5000.

3.1.4. Surface Profiles

Surfaces of PMMA-HAp composite plates were characterized using a surface profilometer. Pure PMMA's surface topography clearly illustrates its smoothness and is quantified with the rms (root mean square) value of 9.797 nm (Figure 3.6). Red lines on the images show the axes along which the topography was analyzed and expressed as histograms. Histograms show that as the highest peak on the PMMA surface is ca 0.015 μm . This value reached to almost 4 μm when 40% HAp loaded PMMA was studied. The rms value gives an average value of the roughness of the surface making it possible to quantify the roughness. As the hydroxyapatite content was increased, the rms value reached 1049 nm with 40% HAp carrying PMMA sample. This confirms that the roughness of the surfaces increased with increasing HAp content. This was expected and actually targeted because presence of HAp particles would serve as cell attachment sites and also upon dissolution of the crystals as voids for tissue ingrowth. Cell attachment and proliferation, therefore is expected to be higher in rougher surfaces since it is shown that cell adhesion is positively affected by the increasing roughness (Lampin *et al.*, 1996).

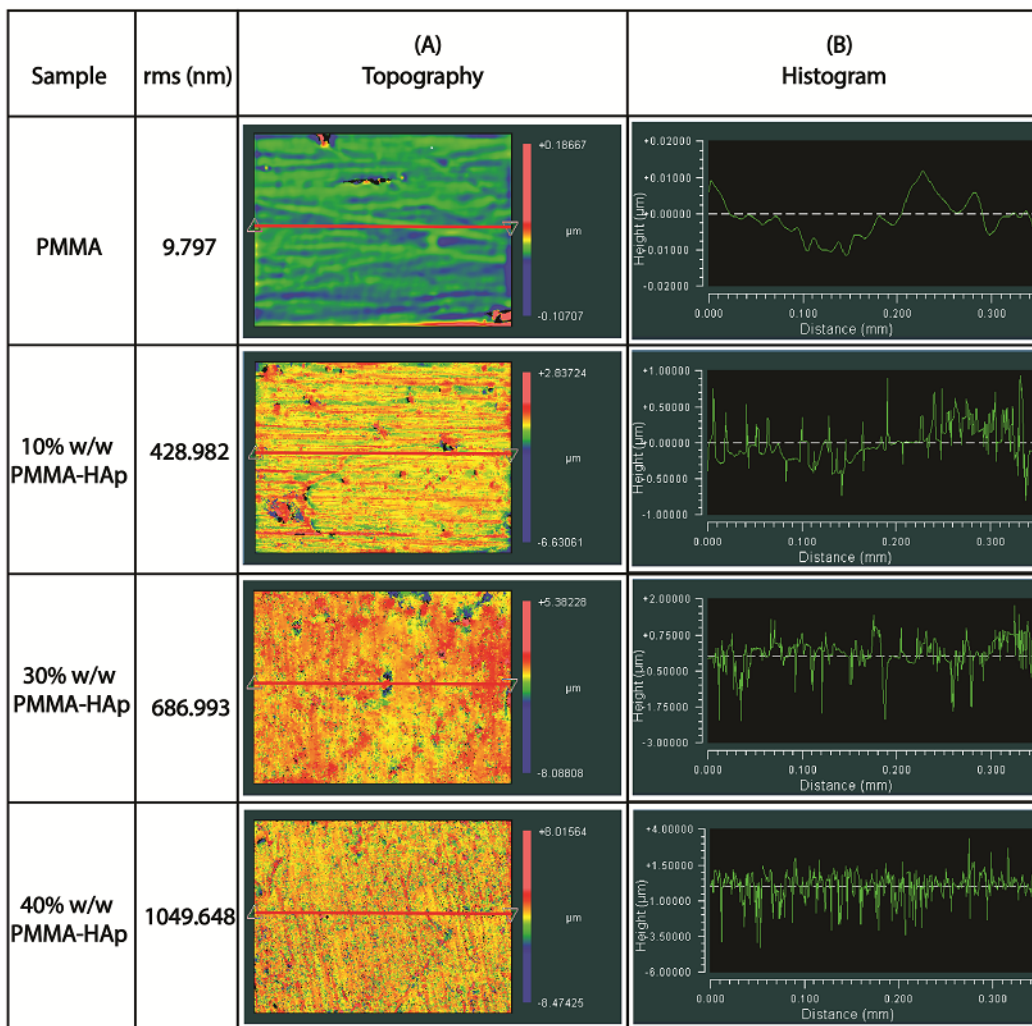


Figure 3.6 Analysis of surface roughness produced by optical surface profiler. (A) Surface topography, (B) histograms of the surfaces with increasing amounts of HAp.

3.1.5. Contact Angle

The results of the contact angle studies (Figure 3.7) show that as the HAp content in PMMA increases, the water contact angle on the sample surfaces also increases. If the surface were perfectly smooth then the increase in the contact angle could have been interpreted as the result of HAp presence as a different chemistry. However, it is known that roughness even with the same chemistry alters the contact angle. The water contact

angle of the pure PMMA plate was $73.2^{\circ} \pm 2.5^{\circ}$, which was the lowest contact angle measured. In the end, maximum contact angle value of $97.6^{\circ} \pm 6.1^{\circ}$ was obtained with the highest HAp content of 40 % (w/w). Although there is a visible increase, the data was statistically significant only between 30-40% HAp content in PMMA ($p < 0.05$). Jung and Bhushan (2006) investigated the effect of surface roughness of modified PMMA on its wettability, and they theoretically and experimentally showed that the surface roughness increased the contact angle on the surfaces. The profilometer data presented in the section 3.1.4, had also shown that the surface roughness of the plates increased in parallel with the HAp content, which is the reason why the contact angle of water increased with increasing HAp content in PMMA instead of decreasing.

Tihan *et al.*, (2009) studied the biocompatibility of PMMA-HAp composites and characterized them using contact angle studies. They found that the water contact angle decreased from 97° with PMMA to 68° with a HAp content of 15 % (w/w). The reason that they observed a decrease in the water contact angle with HAp addition may be the result of the differences in preparation methods. They polymerized the monomer in NH_4OH solution and incorporated HAp into the structure during the process. The initial contact angle of PMMA was much higher than the value obtained in this study indicating a completely different surface chemistry. Besides, there is the question of surface roughness of their samples. Therefore, it can be said that the surface characteristics are affected by the processing methods.

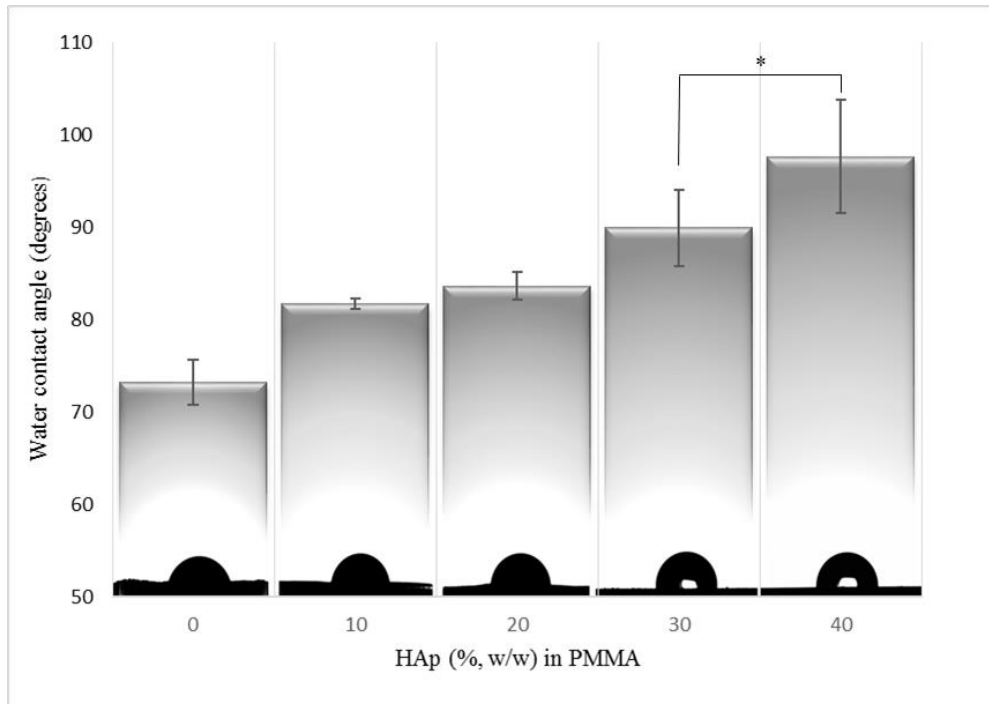


Figure 3.7 Water contact angles for pure PMMA and PMMA-HAp composites.

3.2. *In vitro* Studies

3.2.1. Cell Attachment and Proliferation

Alamar Blue assay yields quantitative results about the adhesive and proliferative behavior of the cells. The data was obtained as the percentage of the reduction of the dye used in the test and the results were then converted into the cell number using a calibration curve (Appendix A) that is prepared with the procedure described in section 2.2.3.3. The results obtained from the assay (Figure 3.8) on Day 1, were used to assess the attachment capability of the cells on the substrate surfaces and the rate of change in time yields the proliferative rate. The data obtained in this study for the Day 1 signify that the initial attachments of the cells after 24 h of cell seeding on the sample plates are similar and somewhat lower than the seeded number as is generally observed and is caused by

insufficient attachment on the foreign surfaces. On Day 3, the cell numbers on most plates further decreased with the highest decrease being on PEEK and PMMA and the rest with the highest HAp leading to the maximum attachment. During the complete culture duration of 2 weeks, the data showed increasing cell numbers except for PEEK and PMMA. This was expected as the HOB cells were reported to respond positively to the calcium phosphate containing surfaces (Salih *et al.*, 2006). Similarly, Rong *et al.* (2015) observed that osteoblast-like MG-63 cells adhere more strongly onto HAp containing surfaces than on PMMA, PLA and their blends. These surfaces also presented higher proliferation with HAp. Thus, it can be concluded that proliferation was positively correlated with the amount of HAp content, though the maximum cell attachment and the proliferation was observed on the plates with the 30% HAp content. The cells on TCPS, the control, were the highest throughout the test period. This suggests that HAp incorporation is very important in cell attachment and proliferation but more than 40% (w/w) may not further increase the proliferation rates of the HOB cells.

Shayan *et al.* (2014) studied the responses of osteoblast (MC3T3) cells on pure PMMA and PMMA/TiO₂ (titanium dioxide) composites treated with ultraviolet (UV) light and observed that the lowest cell attachment and proliferation was with pure PMMA samples. Wang *et al.* (2014) reported that the viability of MG-63 cells decreased in PEEK samples compared to PEEK-nano-FHA (nano-fluorohydroxyapatite) composites after 7 days of culture. They also concluded that the cell attachment was increased with increasing roughness of the surfaces.

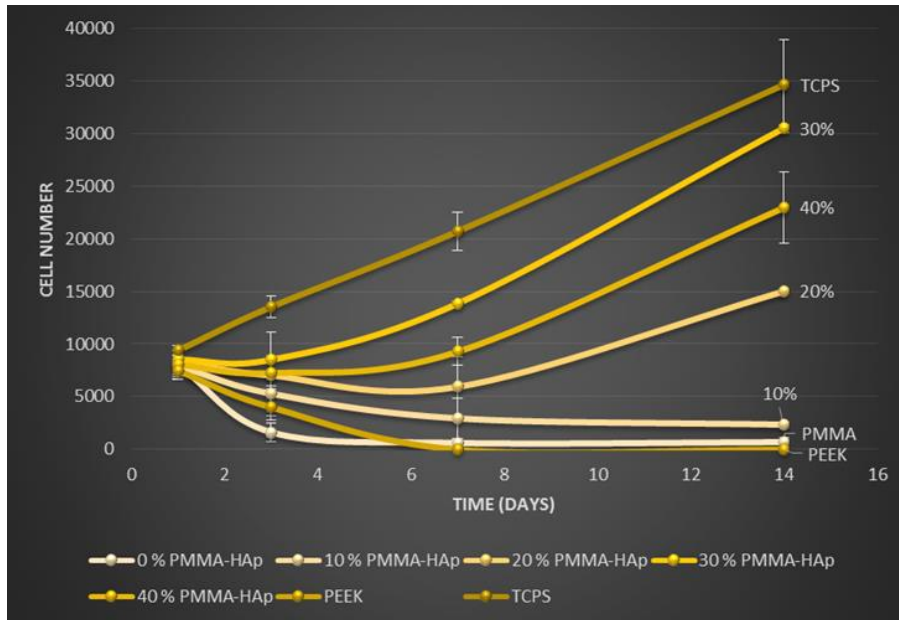


Figure 3.8 Attachment and proliferation of HOB cells on pure PMMA and PMMA-HAp composite plates over 14 days obtained by using the Alamar Blue test. Cell density seeded: 10^4 cells/cm².

Proliferation study could have been conducted using MTT Cell Viability Test more accurately than the Alamar Blue assay because it is not sensitive below the cell number of 5,000. However, the high number of samples and cells required for MTT assay (at every test the specific samples has to be terminated) was a restriction.

Cell attachment on the substrates is reported to be negatively correlated with the increase in hydrophobicity (Wei *et al.*, 2009) even though there are other studies which show a contact angle around 60° is optimum. The incorporation of HAp decreases wettability but increases the roughness as explained in sections 3.1.4 and 3.1.5, and these compensate the decrease in cell adhesion resulting from the level of non-wettability.

3.2.2. Cell Morphology and Spreading

3.2.2.1. Scanning Electron Microscopy and Energy Dispersed X-Ray (EDX)

Analysis

Roughness as well as the linear tracks on the PMMA surfaces formed during processing should be kept in mind when assessing the responses of the cells and SEM is an important tool in studying this situation. SEM micrographs of pure PMMA and 20% (w/w) PMMA-HAp composite plates with and without HOB cells are presented in Figure 3.9. On pure PMMA plates, cells are clearly visible both on Days 3 and 7. On both days, cells were extended, and on the 7th day, one cell is seen to follow the groove that probably was produced by the injection molding process (Figure 3.9C). The cells on the plates with 20% (w/w) HAp content are not easily recognized due to the fact that seeded and unseeded plates are very similar in the micrographs. Energy dispersed X-ray (EDX) analysis, on the other hand, showed that there was no trace of calcium or phosphate on unseeded pure PMMA plates but after seeding with HOB cells a Ca:P ratio of 1.60 was measured possibly due to mineral formation by the bone cells, HOBs. The Ca:P ratio was 1.83 with unseeded 20% PMMA-HAp plates and this number was 1.66 after 7 days of seeding with HOB. As the typical Ca:P ratio of hydroxyapatite (HAp) is 1.67, results show that on pure PMMA, CaP is formed by the cells while for HAp loaded sample, the CaP is present because of the HAp and the new CaP deposited by the cells (Figure 3.10).

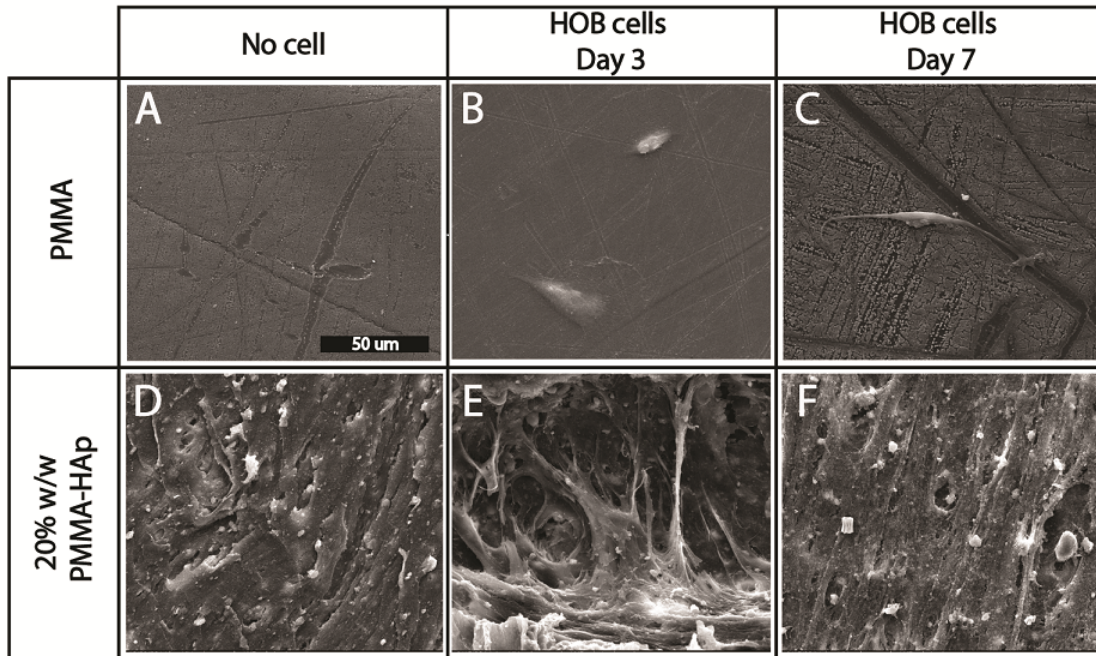


Figure 3.9 SEM micrographs of pure PMMA and 20% (w/w) PMMA-HAp composite plates. The plates are without (A, D) and with (B-C, E-F) HOB cells on (B, E) day 3 and (C, F) day 7. Cell density: 5000 cells/cm². Upper row; (A-C) pure PMMA plates and lower row; (D-F) 20% (w/w) PMMA-HAp composite plates. Mag. X2000 for all.

It was reported that both the roughness and the patterns on the surface affect the attachment and alignment as well as the proliferation rate of the cells and this influence depends on the type of the cells used (Jeon *et al.*, 2014). Jeon *et al.*, (2012) reported higher calcium deposition and increased osteoblast viability on rougher surfaces of PCL than smoother ones. Also, surfaces with micron sized grooves and with patterns have been reported to lead to strong elongation and alignment of osteoblast cells on polyimide surfaces, and increased alignment and spreading of mouse osteoblastic cells on PET films (Charest *et al.*, 2004; Chollet *et al.*, 2010, respectively).

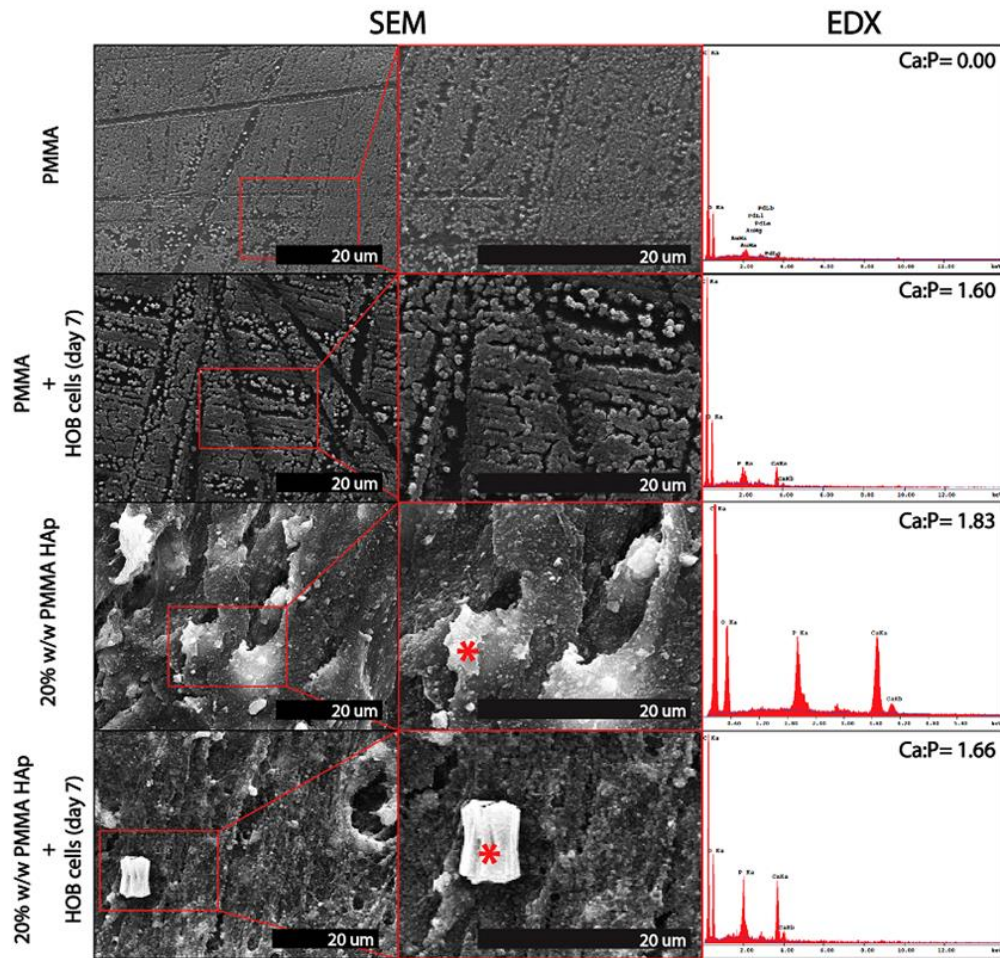


Figure 3.10 Energy dispersed X-ray (EDX) analysis of pure PMMA and 20% PMMA-HAp plates with and without HOB cells. Cell culture time: 7 days.

3.2.2.2. Confocal Laser Scanning Microscopy (CLSM) Analysis

In order to study the morphologies of the cells and to assess their level of contact with the surfaces bone cell line, HOB cells, were seeded (at the density of 10^4 cells/cm²) onto pure PMMA and PMMA-HAp composite plates. After 3 and 7 days, the cells were observed with CLSM and the results are presented in Figure 3.11. It is observed that the normal, needle-like morphology of the HOB cells is preserved on pure PMMA plates. Also, they

show an alignment with each other which can be attributed to the nature of the surface resulting from the processing conditions (the streaks and lines resulting from the injection molding). On the other hand, on the composite plates, 20 % (w/w) and 40 % (w/w), no such alignment was observed (Figure 3.11). Instead, the cells were spread and many filopodia could be seen which can be attributed to the higher interaction between the cells and the surface and also preferential attachment of the HOB cells to HAp particles which may have surfaced and created a rougher surface. Dalby *et al.* (2002) observed similar results that as the amount of HAp in PMMA increases up to 8.8 % (v/v), the number of focal adhesion plaques also increased leading to a greater actin cytoskeleton organization with many filopodia in bundles.

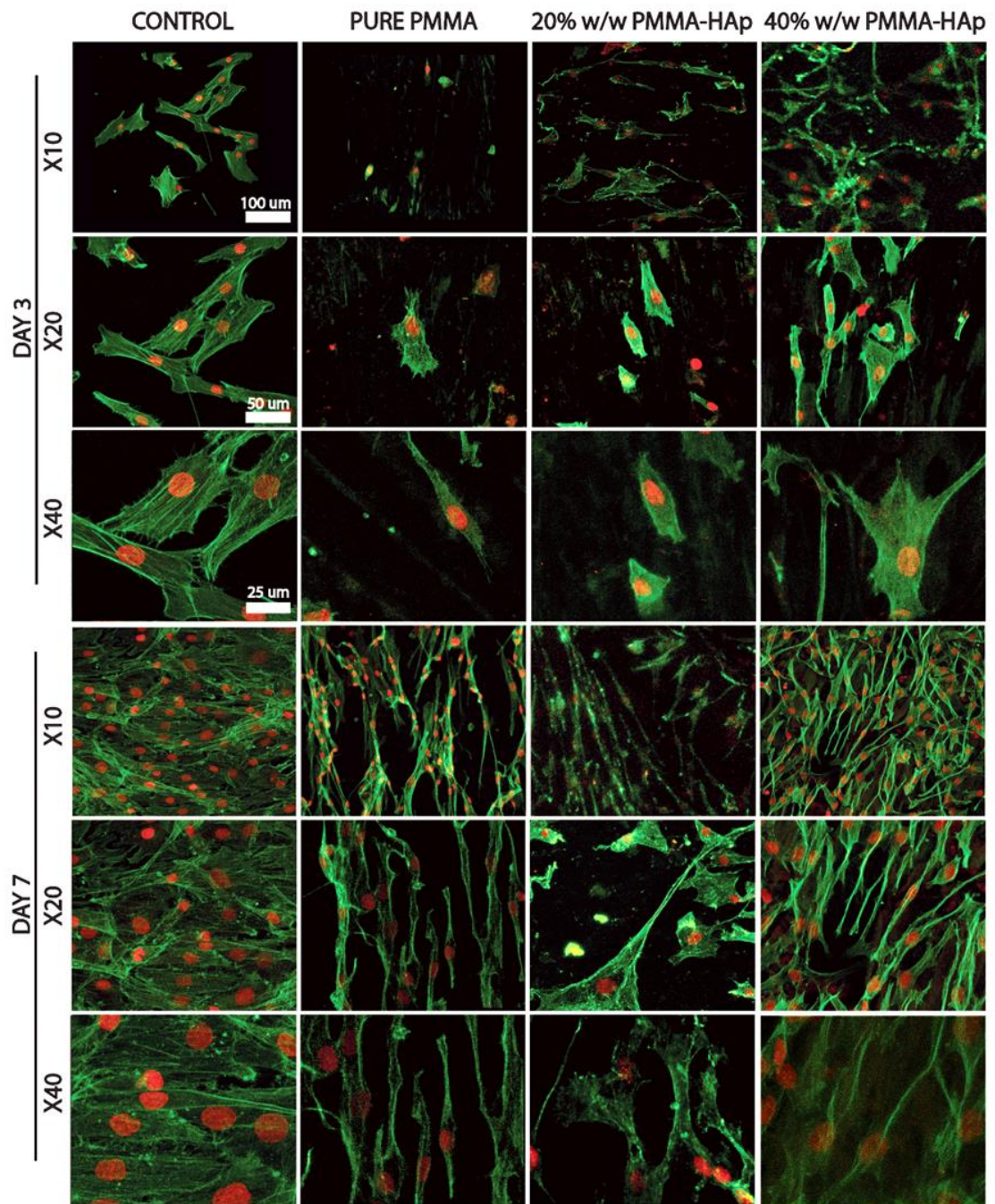


Figure 3.11 CLSM images of HOB cells on pure PMMA and on 20% and 40% PMMA-HAp composite plates on Day 3 and 7. Cells were stained with FITC-phalloidin (green) for the actin of the cytoskeleton and DRAQ5 (red) for the nuclei.

On Day 7 of the cell culture, the cells on the 40 % (w/w) PMMA-HAp plates achieved a significantly more surface coverage than on the pure PMMA or the 20 % (w/w) PMMA-HAp plates, which is consistent with the Alamar Blue assay results presented in Figure 3.8. This result is also supported by Xing *et al.* (2013) who used nanofibrous PMMA scaffolds loaded with HAp and found that cell morphology and adhesion is related with the cytoskeletal organization which, in turn, is affected positively by the increase in HAp content. Figure 3.12 illustrates the filopodia formed by the HOB cells on plates with 40% HAp and cell that have stretched to at least 482 μm . All this, therefore, suggests that HOB cells have a preference for PMMA implants with embedded HAp particles in their adhesion, proliferation and spreading.

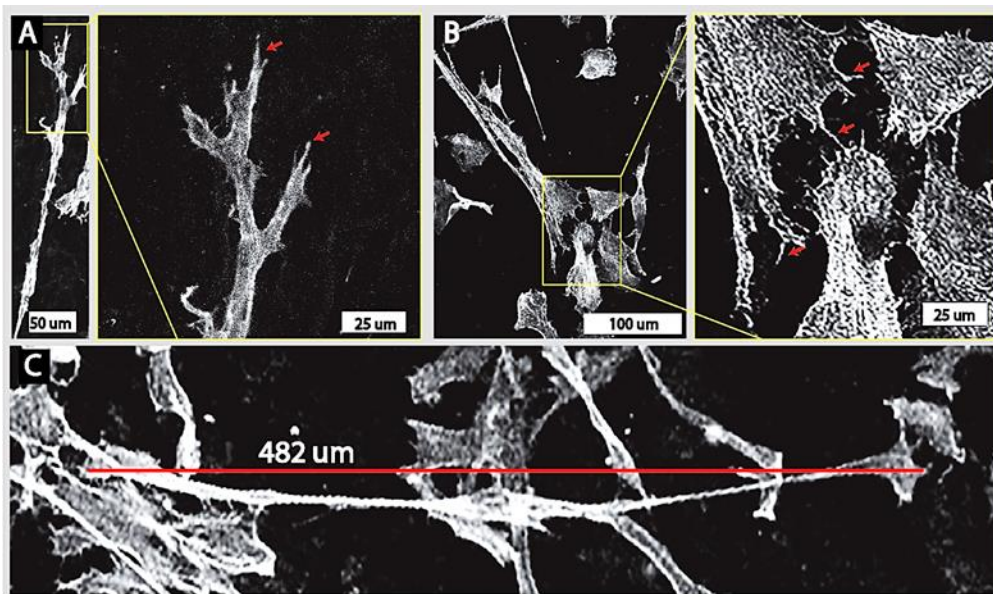


Figure 3.12 Representative CLSM images of HOB cells. (A, B) The filopodia and (C) elongation of HOB cells were observed on plates with 40% (w/w) HAp in PMMA on Day 7.

3.2.3. Staining of Calcium

Qualitative results of staining calcium with Alizarin Red are presented in Figure 3.13. The method is a widely used method to detect/qualify the presence of the calcium either produced by the cells or present due to the HAP-incorporated composite plates themselves. For the unseeded samples, a gradient can be observed in the plates as the HAp content gradually increases. As for the plates seeded with HOB cells, after the 14th day of the culture, the presence of the cells on the plates are clearly marked with the red dye.

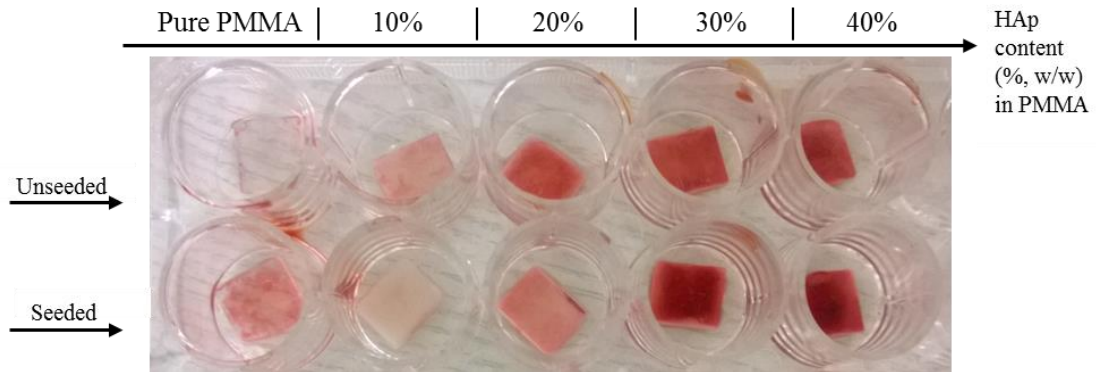


Figure 3.13 Staining of Ca^{+2} with Alizarin Red of PMMA and PMMA-HAp plates, with and without cells. Upper row: unseeded, lower row: seeded plates (cell density: 10^4 cells/cm²). Cell seeded samples are cultured for 14 days

CHAPTER 4

CONCLUSION

Lumbar region of the spine can suffer deformities and disorders that can be caused by age, trauma or genetic reasons. Spondylosis and degenerative disc disease are among these. Where non-operative treatments are no longer optional, such problems are surgically treated by means of fusing the vertebral bodies to each other. The devices used in these procedures include screws, plates and cages. There are many commercially available spinal fusion cages made of metals (e.g. titanium) and polymers (e.g. PEEK). The designs, as well as the materials, of these cages that have a significant effect on the outcome of the surgery.

Poly(methylmethacrylate) (PMMA) is a synthetic polymer that is used for many years in orthopedic implants as bone plates, fillers and cements. However, the mechanical properties and the cell-material interactions are not suitable for a proper performance as spinal fusion cages.

In this study, hydroxyapatite (HAp) was incorporated into PMMA in varying proportions using hot melt extrusion followed by injection molding. The specimens were characterized mechanically and with *in vitro* tests using human osteoblast-like (HOB) cells, and the behavior of the HOB cells on these new, modified surfaces were studied.

The mechanical properties of the pure PMMA and PMMA-HAp composite specimens showed a significant improvement in the elastic modulus, increased in tension with samples having up to 40% (w/w) HAp amount and in compression with samples having 20% (w/w) HAp in PMMA. Ultimate tensile strength did not show any increase though

compressive strength increased with samples that have up to 20% HAp content in PMMA and then the rate of increase leveled off. These showed that the mechanical properties were significantly improved.

Scanning electron microscopy and optical surface profilometry studies of PMMA showed that the surface roughness increased with increasing HAp content. Water contact angles of these surfaces also showed an increase.

The attachment, proliferation and the morphological changes of the HOB cells in response to these surfaces were also evaluated using Alamar Blue assay, SEM and CLSM. The results suggested that as the HAp is increased within the PMMA matrix, cell attachment within 3 days and proliferation over 14 days also increased. Besides, the cells presented changes in the morphology producing filopodia with plates with high amounts of HAp. These suggested that cell-material interaction were also improved.

All these suggest that PMMA and HAp can be successfully compounded and, have suitable mechanical strength that can carry the load to which the spine is subjected and have improved cell-material interaction that could lead to a better fusion in the lumbar spine. Thus, the high HAp content PMMA samples could be a new material for spinal fusion applications.

REFERENCES

- Abbah, S., Lam, C. X. L., Hutmacher, D. W., Goh, J. C. H., & Wong, H.-K. (2009). Biological performance of a polycaprolactone-based scaffold used as fusion cage device in a large animal model of spinal reconstructive surgery. *Biomaterials*, 30(28), 5086–93.
- Agazzi, S., Reverdin, A., & May, D. (1999). Posterior lumbar interbody fusion with cages: an independent review of 71 cases. *Journal of Neurosurgery: Spine*, 91(2), 186-192. Outcomes Research Trial (SPORT). *Spine*, 35(14), 1329.
- Ali, U., Karim, K. J. B. A., & Buang, N. A. (2015). A Review of the Properties and Applications of Poly (Methyl Methacrylate) (PMMA). *Polymer Reviews*, 55(4), 678-705.
- Andersson, G. B., & Frymoyer, J. W. (1997). *The Adult Spine: Principles and Practice*.
- Arabmotlagh, M., Bachmaier, S., Geiger, F., & Rauschmann, M. (2014). PMMA-hydroxyapatite composite material retards fatigue failure of augmented bone compared to augmentation with plain PMMA: In vivo study using a sheep model. *Journal of Biomedical Materials Research Part B: Applied Biomaterials*, 102, 1613–1619.
- American Society for Testing and Materials, Standard 638 (2010) Standard test method for tensile properties of plastics. *Annual Book of ASTM Standards*, West Conshohocken, PA
- Bagby GW. (1988). Arthrodesis by the distraction-compression method using a stainless steel implant. *Orthopedics*, 11, 931–934
- Boger, A., Wheeler, K., Montali, A., & Gruskin, E. (2009). NMP-modified PMMA bone cement with adapted mechanical and hardening properties for the use in cancellous bone augmentation. *Journal of Biomedical Materials Research Part B: Applied Biomaterials*, 90(2), 760-766.
- Bono, C. M., & Lee, C. K. (2004). Critical analysis of trends in fusion for degenerative disc disease over the past 20 years: influence of technique on fusion rate and clinical outcome. *Spine*, 29(4), 455-463.
- Brenke, C., Kindling, S., Scharf, J., Schmieder, K., & Barth, M. (2013). Short-term experience with a new absorbable composite cage (β -tricalcium phosphate–polylactic acid) in patients after stand-alone anterior cervical discectomy and fusion. *Spine*, 38(11), E635-E640.

Brenke, C., Pott, P. P., Schwarz, M. L., Schmieder, K., & Barth, M. (2014). Development of a low-cost Polymethylmethacrylate (PMMA) stand-alone cervical cage: technical note. *Journal of Neurological Surgery*, 75(4), 317-322.

Browner B., Jupiter J., Levine A., Trafton P. (1998). *Skeletal Trauma 2nd Edition*, W.B. Saunders, 101.

Buckwalter, J., Glimcher, M., Cooper, R., & Recker, R. (1995). Bone biology. *J Bone Joint Surg Am*, 1256–1275.

Byrne, T., Benzel, E., & Waxman, S. (2000). Degenerative disorders of the spine. In: *Diseases of the Spine and Spinal Cord*, 124-165. New York: Oxford University Press.

Cahill, K. S., McCormick, P. C., & Levi, A. D. (2015). A comprehensive assessment of the risk of bone morphogenetic protein use in spinal fusion surgery and postoperative cancer diagnosis. *Journal of Neurosurgery: Spine*, 1-8.

Callister, W. D., & Rethwisch, D. G. (2007). Characteristics, applications and processing of polymers. In: *Materials Science and Engineering: An Introduction*, 524-532. New York: John Wiley and Sons, Inc.

Chen, J. F., Wu, C. T., Lee, S. C., & Lee, S. T. (2005). Use of a polymethylmethacrylate cervical cage in the treatment of single-level cervical disc disease. *Journal of Neurosurgery: Spine*, 3(1), 24-28.

Currey, J. D. (1998). Mechanical properties of vertebrate hard tissues. *Proceedings of the Institution of Mechanical Engineers, Part H: Journal of Engineering in Medicine*, 212(6), 399-411.

Dalby, M. J., Di Silvio, L., Harper, E. J., & Bonfield, W. (2002). Increasing hydroxyapatite incorporation into poly(methylmethacrylate) cement increases osteoblast adhesion and response. *Biomaterials*, 23(2), 569–576.

Dhoble, A., Padole, P., & Dhoble, M. (2012). Bone Mechanical Properties : A Brief Review, *Trends in Biomaterials and Artificial Organs*, 26(1), 25-30.

Fairbank, J., Frost, H., Wilson-MacDonald, J., Yu, L. M., Barker, K., & Collins, R. (2005). Randomised controlled trial to compare surgical stabilisation of the lumbar spine with an intensive rehabilitation programme for patients with chronic low back pain: The MRC spine stabilisation trial. *BMJ: British Medical Journal*, 330(7502), 1233.

Farrokhi, M. R., Nikoo, Z., Gholami, M., & Hosseini, K. (2015). Comparison between acrylic cage and polyetheretherketone (PEEK) cage in single-level anterior cervical discectomy and fusion: A randomized clinical trial. *Journal of Spinal Disorders & Techniques*. Abstract retrieved from http://journals.lww.com/jspinaldisorders/Abstract/publishahead/Comparison_between_Acrylic_Cage_and.99121.aspx

- Farrokhi, M. R., Torabinezhad, S., & Ghajar, K. A. (2010). Pilot study of a new acrylic cage in a dog cervical spine fusion model. *Journal of Spinal Disorders & Techniques*, 23(4), 272-277.
- Goldstein, S. A., Matthews, L. S., Kuhn, J. L., & Hollister, S. J. (1991). Trabecular bone remodeling: an experimental model. *Journal of Biomechanics*, 24, 135-150.
- Hamburger, C., Festenberg, F. V., & Uhl, E. (2001). Ventral discectomy with PMMA interbody fusion for cervical disc disease: long-term results in 249 patients. *Spine*, 26(3), 249-255.
- Hanc, M., Fokter, S. K., Vogrin, M., Molicnik, A., & Recnik, G. (2015). Porous tantalum in spinal surgery: an overview. *European Journal of Orthopaedic Surgery & Traumatology*, 1-7.
- Harper, C. A. (Ed.). (2000). Chapter 11 Plastics testings. In: *Modern Plastics Handbook*, 11.1-11.94. New York: McGraw-Hill Companies Inc.
- Hench, L. L., & Wilson, J. (1993). Introduction. In: *An Introduction to Bioceramics*, 1-23. Singapore World Scientific Publishing Co. Pte. Ltd.
- Holthaus, M. G., Treccani, L., & Rezwan, K. (2012). Osteoblast viability on hydroxyapatite with well-adjusted submicron and micron surface roughness as monitored by the proliferation reagent WST-1. *Journal of Biomaterials Applications*, 27(7), 791–800.
- Ito, M., Onodera, T., & Funakoshi, T. (2015). Metallic Biomaterials in Orthopedic Surgery. *Advances in Metallic Biomaterials*, 213-231.
- Kang, B., Chak, S., & Chae, H. (2012). A study of the use of a hydroxyapatite and poly(methyl methacrylate) composite as a material for implants. *Journal of Ceramic Processing Research*, 13(6), 791-796.
- Keaveny, T. M., & Hayes, W. C. (1993). Mechanical properties of cortical and trabecular bone. *Bone*, 7, 285-344.
- Kerr 3rd, E. J., Jawahar, A., Wooten, T., Kay, S., Cavanaugh, D. A., & Nunley, P. D. (2010). The use of osteo-conductive stem-cells allograft in lumbar interbody fusion procedures: an alternative to recombinant human bone morphogenetic protein. *Journal of Surgical Orthopaedic Advances*, 20(3), 193-197.
- Kini, U., & Nandeesh, B. N. (2012). Physiology of bone formation, remodeling, and metabolism. *Radionuclide and Hybrid Bone Imaging*, 29-57.
- Kurtz, S. M., & Devine, J. N. (2007). PEEK biomaterials in trauma, orthopedic, and spinal implants. *Biomaterials*, 28(32), 4845–69.

Lampli, J., Whitaker, M. C., Moskowitz, A., Duong, J., Dong, F., Felts, L & Wooley, P. (2014). Stand-alone anterior lumbar interbody fusion for degenerative disc disease of the lumbar spine: results with a 2-year follow-up. *Spine*, 39(15), E894-E901.

Lampin, M., Warocquier-Clérout, R., Legris, C., Degrange, M., & Sigot-Luizard, M. F. (1997). Correlation between substratum roughness and wettability, cell adhesion, and cell migration. *Journal of Biomedical Materials Research*, 36(1), 99-108.

Lequin, M. B., Verbaan, D., & Bouma, G. J. (2014). Posterior lumbar interbody fusion with stand-alone Trabecular Metal cages for repeatedly recurrent lumbar disc herniation and back pain: Clinical article. *Journal of Neurosurgery: Spine*, 20(6), 617-622.

Lin, C. Y., Wirtz, T., LaMarca, F., & Hollister, S. J. (2007). Structural and mechanical evaluations of a topology optimized titanium interbody fusion cage fabricated by selective laser melting process. *Journal of Biomedical Materials Research Part A*, 83(2), 272-279.

Lipson, S. J., & Muir, H. (1981). Proteoglycans in Experimental Intervertebral Disc Degeneration. *Spine*, 6(3), 194-210.

Martin, B. I., Lurie, J. D., Deyo, R. A., Tosteson, A. N., Farrokhi, F., & Mirza, S. K. (2014). Trends in the use of bone morphogenetic protein among patients undergoing fusion for degenerative diagnoses in the United States, *Spine Journal Meeting Abstracts*, 15-16.

Mellon, S. J., & Tanner, K. E. (2012). Bone and its adaptation to mechanical loading: a review. *International Materials Reviews*, 57(5), 235–255.

Mirza, S. K., & Deyo, R. A. (2007). Systematic review of randomized trials comparing lumbar fusion surgery to non-operative care for treatment of chronic back pain. *Spine*, 32(7), 816-823.

Moreno, K., Garcia-Miranda, J., Hernandez-Navarro, C., Ruiz-Guillen, F., Aguilera-Camacho, L., Lesso, R., & Arizmendi-Morquecho, a. (2015). Preparation and performance evaluation of PMMA/HA nanocomposite as bulk material. *Journal of Composite Materials*, 49, 1345–1353.

Nyman, J. S., Roy, A., Shen, X., Acuna, R. L., Tyler, J. H., & Wang, X. (2006). The influence of water removal on the strength and toughness of cortical bone. *Journal of Biomechanics*, 39(5), 931–8.

Ohtori, S., Koshi, T., Yamashita, M., Yamauchi, K., Inoue, G., Suzuki, M., & Takahashi, K. (2011). Surgical versus nonsurgical treatment of selected patients with discogenic low back pain: a small-sized randomized trial. *Spine*, 36(5), 347-354.

- Park, J., & Lakes, R. S. (2007). Hard tissue replacements-II: Joints and teeth. In: *Biomaterials: An Introduction*, 395-458. New York: Springer Science & Business Media.
- Pereira, D. R., Silva-Correia, J., Oliveira, J. M., & Reis, R. L. (2013). Hydrogels in acellular and cellular strategies for intervertebral disc regeneration. *Journal of Tissue Engineering and Regenerative Medicine*, 7(2), 85–98.
- Ray, C. D. (1997). Threaded titanium cages for lumbar interbody fusions. *Spine*, 22(6), 667-679.
- Roeder, R. K., Smith, S. M., Conrad, T. L., Yanchak, N. J., Merrill, C. H., & Converse, G. L. (2009). Porous and bioactive PEEK implants for interbody spinal fusion. *Adv. Mater. Process*, 167, 46-48.
- Rong, Z., Zeng, W., Kuang, Y., Zhang, J., Liu, X., Lu, Y., & Cheng, X. (2015). Enhanced bioactivity of osteoblast-like cells on poly(lactic acid)/poly(methyl methacrylate)/nanohydroxyapatite scaffolds for bone tissue engineering. *Fibers and Polymers*, 16(2), 245–253.
- Rutherford, E. E., Tarplett, L. J., Davies, E. M., Harley, J. M., & King, L. J. (2007). Lumbar Spine Fusion and Stabilization: Hardware, Techniques, and Imaging Appearances 1. *Radiographics*, 27(6), 1737-1749.
- Saha, S., & Pal, S. (1984). Mechanical properties of bone cement: a review. *Journal of Biomedical Materials Research*, 18(4), 435–62.
- Salih, V., Mordan, N., Abou Neel, E. a., Armitage, D. a., Jones, F. H., Knowles, J. C., Cauich-Rodriguez, J. V. (2006). Surface characterisation of various bone cements prepared with functionalised methacrylates/bioactive ceramics in relation to HOB behaviour. *Acta Biomaterialia*, 2, 143–154.
- Savatier L, Curnier F, K. I. (2014). Article Micro-CT evaluation of cavities prepared with different Er : YAG handpieces. *European Journal of Paediatric Dentistry*, 15(2), 95–100.
- Schimmel, J. J., Poeschmann, M. S., Horsting, P. P., Schönfeld, D. H., van Limbeek, J., & Pavlov, P. W. (2012). PEEK Cages in Lumbar Fusion: Mid-term Clinical Outcome and Radiological Fusion. *Journal of Spinal Disorders & Techniques*. Abstract retrieved from <http://europepmc.org/abstract/med/22907069>.
- Sumner, D. R., Turner, T. M., Igloria, R., Urban, R. M., & Galante, J. O. (1998). Functional adaptation and ingrowth of bone vary as a function of hip implant stiffness. *Journal of Biomechanics*, 31, 909–917.
- Thurner, P. J., Erikson, B., Schriock, Z., Langan, J., Scott, J., Zhao, M., & Hansma, P. K. (2005, January). High-speed photography of human trabecular bone during compression. *MRS Proceedings*, 874, L1-2.

- Tihan, T. G., Ionita, M. D., Popescu, R. G., & Iordachescu, D. (2009). Effect of hydrophilic-hydrophobic balance on biocompatibility of poly(methyl methacrylate) (PMMA)-hydroxyapatite (HA) composites. *Materials Chemistry and Physics*, 118, 265–269.
- Uthoff, H. K., Poitras, P., & Backman, D. S. (2006). Internal plate fixation of fractures: Short history and recent developments. *Journal of Orthopaedic Science*, 11, 118–126.
- Vallo, C. I., Montemartini, P. E., Fanovich, M. A., Lopez, J. M. P., & Cuadrado, T. R. (1999). Polymethylmethacrylate-based bone cement modified with hydroxyapatite. *Journal of Biomedical Materials Research*, 48(2), 150-158.
- van Dijk, M., Smit, T. H., Sugihara, S., Burger, E. H., & Wuisman, P. I. (2002). The effect of cage stiffness on the rate of lumbar interbody fusion: an in vivo model using poly (l-lactic Acid) and titanium cages. *Spine*, 27(7), 682-688.
- Voisin, M., Saunders, F., Yen, D., & Fenton, P. (2015). Evaluation of fusion in a PEEK cage after anterior cervical discectomy and fusion. *Canadian Journal of Neurological Sciences*, 42.
- Wagoner Johnson, A. J., & Herschler, B. a. (2011). A review of the mechanical behavior of CaP and CaP/polymer composites for applications in bone replacement and repair. *Acta Biomaterialia*, 7(1), 16–30.
- Wang, L., He, S., Wu, X., Liang, S., Mu, Z., Wei, J., Wei, S. (2014). Polyetheretherketone/nano-fluorohydroxyapatite composite with antimicrobial activity and osseointegration properties. *Biomaterials*, 35(25), 6758–6775.
- Weber, K. T., Jacobsen, T. D., Maidhof, R., Virojanapa, J., Overby, C., Bloom, O., & Chahine, N. O. (2015). Developments in intervertebral disc disease research: pathophysiology, mechanobiology, and therapeutics. *Current Reviews in Musculoskeletal Medicine*, 8(1), 18-31.
- Wei, J., Igarashi, T., Okumori, N., Igarashi, T., Maetani, T., Liu, B., & Yoshinari, M. (2009). Influence of surface wettability on competitive protein adsorption and initial attachment of osteoblasts. *Biomedical Materials*, 4, 045002.
- Weiner, B. K., & Fraser, R. D. (1998). Lumbar interbody cages. *Spine*, 23(5), 634-640.
- Weinstein, J. N., Tosteson, T. D., Lurie, J. D., Tosteson, A., Blood, E., Herkowitz, H., & An, H. (2010). Surgical versus non-operative treatment for lumbar spinal stenosis four-year results of the Spine Patient Outcomes Research Trial (SPORT). *Spine*, 35(14), 1329.
- Wollowick, A. L., & Sarwahi, V. (Eds.). (2015). Anterior lumbar interbody fusion. In: *Spondylolisthesis: Diagnosis, Non-Surgical Management, and Surgical Techniques*, 179-190. New York: Springer Science & Business Media.

Wozney, J. M. (2002). Overview of bone morphogenetic proteins. *Spine*, 27(16S), S2-S8.

Xing, Z. C., Han, S. J., Shin, Y. S., Koo, T. H., Moon, S., Jeong, Y., & Kang, I. K. (2013). Enhanced osteoblast responses to poly (methyl methacrylate)/hydroxyapatite electrospun nanocomposites for bone tissue engineering. *Journal of Biomaterials Science, Polymer Edition*, 24(1), 61-76.

Yuan, Y., & Lee, T. R. (2013). Contact angle and wetting properties. In: *Surface science techniques*, 3-34. New York: Springer Science & Business Media.

Zebarjad, S. M., Sajjadi, S. A., Sdrabadi, T. E., Sajjadi, S. A., Yaghmaei, A., & Naderi, B. (2011). A Study on Mechanical Properties of PMMA/Hydroxyapatite Nanocomposite. *Engineering*, 3(08), 795.

Zhang, Y., Tanner, K. E., Gurav, N., & Di Silvio, L. (2007). In vitro osteoblastic response to 30 vol% hydroxyapatite-polyethylene composite. *Journal of Biomedical Materials Research Part A*, 81(2), 409-417.

Zhao, Y., Wong, H. M., Wang, W., Li, P., Xu, Z., Chong, E. Y., & Chu, P. K. (2013). Cytocompatibility, osseointegration, and bioactivity of three-dimensional porous and nanostructured network on polyetheretherketone. *Biomaterials*, 34(37), 9264-9277.

APPENDIX A

STANDARD CURVE FOR ALAMAR BLUE ASSAY OF HOB CELLS

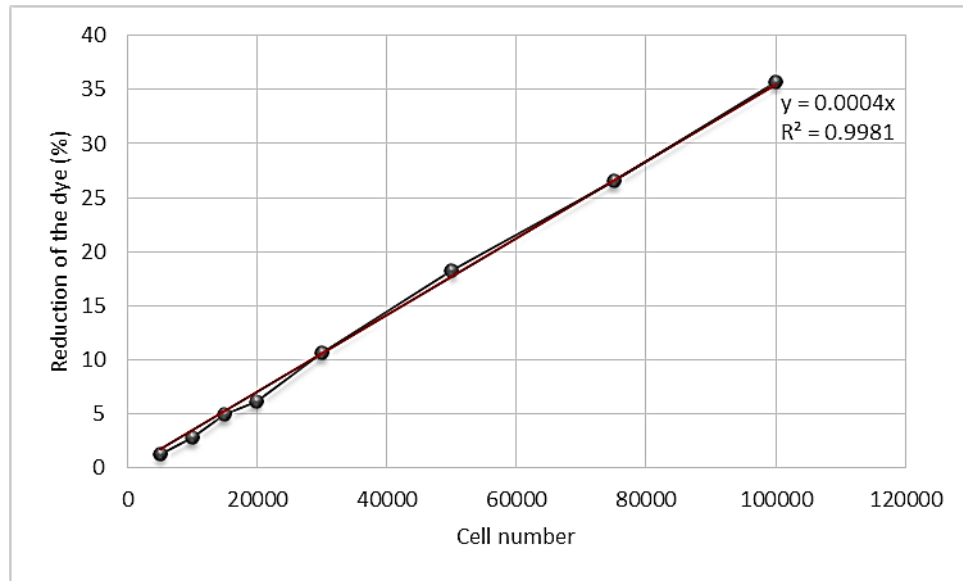


Figure A.1 Standard curve for Alamar Blue assay for human osteoblast (HOB) cells.